Bifurcation analysis of a normal form for excitable media: Are stable dynamical alternans on a ring possible?

Georg A. Gottwald[a)]
School of Mathematics and Statistics and Centre for Mathematical Biology, University of Sydney, Sydney, NSW 2006, Australia

(Received 20 March 2007; accepted 12 February 2008; published online 27 March 2008)

We present a bifurcation analysis of a normal form for traveling waves in one-dimensional excitable media. The normal form that has been recently proposed on phenomenological grounds is given in the form of a differential delay equation. The normal form exhibits a symmetry-preserving Hopf bifurcation that may coalesce with a saddle node in a Bogdanov–Takens point, and a symmetry-breaking spatially inhomogeneous pitchfork bifurcation. We study here the Hopf bifurcation for the propagation of a single pulse in a ring by means of a center manifold reduction, and for a wave train by means of a multiscale analysis leading to a real Ginzburg–Landau equation as the corresponding amplitude equation. Both the center manifold reduction and the multiscale analysis show that the Hopf bifurcation is always subcritical independent of the parameters. This may have links to cardiac alternans, which have so far been believed to be stable oscillations emanating from a supercritical bifurcation. We discuss the implications for cardiac alternans and revisit the instability in some excitable media where the oscillations had been believed to be stable. In particular, we show that our condition for the onset of the Hopf bifurcation coincides with the well known restitution condition for cardiac alternans. © *2008 American Institute of Physics*.
[DOI: 10.1063/1.2890430]

Excitable media are abundant in nature. Examples range from small-scale systems such as intracellular calcium waves to large-scale systems such as cardiac tissue. There exists a plethora of models describing excitable media, each of those particular to the microscopic details of the underlying biological, chemical, or physical system. However, excitable media have certain features that are common to all these systems. In a recent paper, we introduced a normal form for traveling waves in one-dimensional excitable media that contains all bifurcations occurring in excitable media. The normal form consists of a delay-differential equation and is applicable to systems that are close to the saddle-node bifurcation of the traveling wave. Although the normal form has so far only been proposed on phenomenological grounds and has not yet been rigorously derived, its parameters could be successfully fitted to some real excitable media with good quantitative agreement. In this work, we perform a bifurcation analysis of the occurring Hopf bifurcation. This may have important consequences for cardiac dynamics and the understanding of arrhythmias, in particular of alternans. Alternans describe the scenario in cardiac tissue whereby action potential durations are alternating periodically between short and long periods. There is an increased interest in alternans because they are believed to trigger spiral wave breakup in cardiac tissue and to be a precursor to ventricular fibrillation. Up to now, these alternans have been believed to be stable. However, within the normal form we show that the Hopf bifurcation is actually subcritical, suggesting that the resulting oscillations may be unstable.

I. INTRODUCTION

Examples of excitable media are frequently found in biological and chemical systems. Prominent examples are cardiac and neural tissue,[1,2] slime mold colonies in a starving environment,[3] and intracellular calcium waves.[4] There are two defining features of excitable media that are crucial to enable effective signal transmission in biological systems such as cardiac or neural tissue: threshold behavior and relaxation to a stable rest state. The threshold behavior assures that only for large enough stimuli is a signal produced whereas small perturbations decay immediately. For superthreshold perturbations, a signal will decay only after a long excursion—called action potential in the context of cardiac dynamics—back to its stable rest state. This relaxation allows for repeated stimulation, which is essential for wave propagation in cardiac and neural tissue.

Typical solutions in one-dimensional excitable media are wave trains. The wavelength L can range from $L=\infty$ corresponding to an isolated pulse to a minimal value L_c below which propagation fails. Besides wave trains, rotating spiral waves may form in two-dimensional excitable media, and scroll waves in three-dimensional excitable media.[5–9] In the context of cardiac excitable media, propagation failure of these solutions is often linked to clinical situations. In particular, the breakup of spiral waves has been associated with pathological cardiac arrhythmias.[10] Spiral waves may be created in cardiac tissue when wave trains propagate through

a)Electronic mail: gottwald@maths.usyd.edu.au.
This paper is dedicated to Lorenz Kramer; remembering and missing his enthusiasm and creative mind.

inhomogeneities of the cardiac tissue. A reentrant spiral may move around an anatomical obstacle or around a region of partially or totally inexcitable tissue. Once created, they drive the heart at a rate much faster than normal sinus rhythm and cause tachycardia. If these spiral waves then subsequently break up into multiple drifting and meandering spirals and disintegrate into a disorganized state, fibrillation may occur with a possible fatal result for the patient, especially when occurring in the ventricles. It is therefore of great interest to understand the transition from one reentrant spiral to the disorganized collection of complex reentrant pathways. Rather than investigating the full two-dimensional problem of spiral wave breakup which would include interactions of numerous wave arms, one can study some aspects of spiral wave breakup by looking at a one-dimensional slice of a spiral, i.e., at a one-dimensional wave train.[11] A pulse circulating around a one-dimensional ring constitutes the simplest model for a spiral rotating around an anatomical obstacle. Such models concentrate solely on the dynamics close to the anatomical obstacle and ignore the influence of the dynamics of the spiral arms.

Experimentally this problem has been studied since the beginning of the last century. In Ref. 13, the circulation of an electrical pulse around a ring-shaped piece of atrial cardiac tissue from a tortoise heart was investigated as a model for reentrant activity. Recently, the experiments in Ref. 14 investigated the dynamics of pulse circulation around a ring-shaped piece of myocardial tissue from a dog heart. Remarkably, it was found that oscillations of the circulation period of the pulse occurred leading to conduction block and subsequent termination of reentry.

This indicates that a one-dimensional oscillatory instability, named alternans, may be the mechanism triggering spiral wave breakup.[15,11,16–18] This instability occurs when the circulation time of the pulse around the ring is below a certain specific threshold. Below this threshold, alternans arise and action potential durations alternate periodically between short and long periods. We make here the distinction between alternans that are mediated by external periodic stimulations[19–27] and alternans that have a purely dynamical origin. We call the latter ones *dynamical alternans*. It is these dynamical alternans with which this paper is concerned. We will analyze dynamical alternans using a normal form proposed in Ref. 28 for traveling waves in one-dimensional excitable media. The stability of dynamical alternans will be determined by a center manifold theory and by multiple scale analysis. Typically oscillatory instabilities arise in one-dimensional media via Hopf bifurcations. These Hopf bifurcations may be supercritical, resulting in sustained stable oscillations or subcritical leading to a collapse of the oscillations and possibly of the pulse solution. Alternans are widely believed to originate via a supercritical bifurcation.[11,17,29,30] This belief is based on numerical simulations of certain models for cardiac dynamics. However, we note that the above-mentioned experiments[13,14] show that the occurrence of oscillations leads to a subsequent termination of the pulse, which is not suggestive of a supercritical bifurcation.

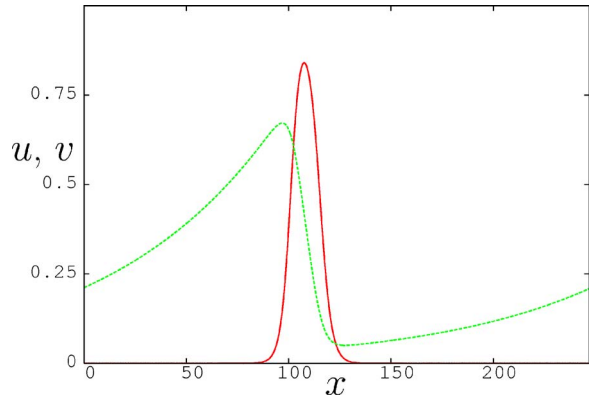

FIG. 1. (Color online) Plot of the activator u (continuous line) and the inhibitor v (dashed line) for the modified Barkley system (70) showing how the activator u weakly interacts with the exponentially decaying tail of the inhibitor v. The parameters are $a=0.22$, $u_s=0.1$, $\epsilon=0.03755$. The ring length is $L=245$, which is close to the critical value L_c for the saddle-node bifurcation.

Our main result for a single pulse and for a wave train in a ring is that in the framework of our normal form, alternans arise as a subcritical Hopf bifurcation. This result is in contrast to the common belief that alternans are stable oscillations. We corroborate our result by numerical simulations of a model for cardiac tissue in which previous numerical simulations suggested the occurrence of stable oscillations. We will see that previous numerical experiments have not been performed sufficiently long to reveal the subcritical character of the Hopf bifurcation. The subcritical character is in agreement with the above-mentioned experiments[13,14] and may explain why alternans often trigger spiral wave breakup and are associated with cardiac failures. The normal form describes excitable media in parameter regions where the system is close to the saddle-node of the traveling wave. This is the case for models such as the FitzHugh–Nagumo model,[31] and is typically the case when the Hopf bifurcation occurs close to the saddle-node bifurcation of the isolated pulse. In particular, the normal form is valid for those classes of excitable media (or parameter regions of a particular excitable medium) where the activator weakly interacts with the preceding inhibitor, which exponentially decays toward the homogeneous rest state. However, for other models such as the model by Echebarria and Karma,[21] there exist parameter regions where upon decreasing the length of the ring, the pulse solution is driven away from the solitary pulse solution and does not weakly interact with the inhibitor. Our normal form cannot describe these oscillations, and we present numerical simulations where oscillations are indeed stable in Sec. V C.

Recently, we have constructed a normal form for traveling waves in one-dimensional excitable media that takes the form of a delay differential equation[28] [see Eqs. (1) and (3)]. The construction is based on the well-known observation that the interaction of a pulse with the inhibitor of the preceding pulse modifies the generic saddle-node bifurcation of an isolated pulse. In Fig. 1, we illustrate this scenario for a modified Barkley model.[32]

The normal form exhibits a rich bifurcation behavior that we could verify by numerically simulating partial differential

equation models of excitable media. Besides the well known saddle-node bifurcations for isolated pulses and for periodic wave trains, the normal form also exhibits a Hopf bifurcation and a symmetry-breaking, spatially inhomogeneous pitchfork bifurcation. Moreover, the normal form shows that the saddle node and the Hopf bifurcation are an unfolding of a Bogdanov–Takens point as previously suggested in Refs. 33 and 34. The Hopf bifurcation is found to occur before the saddle-node bifurcation for a single pulse in a ring. For a wave train consisting of several pulses in a ring, the Hopf and the saddle-node bifurcations occur after the symmetry-breaking pitchfork bifurcation in which every second pulse dies. We could verify these scenarios in numerical simulations of a modified Barkley model[32] and the FitzHugh–Nagumo equations.[31] The normal form provides a unified framework to study all possible bifurcations of traveling waves in one-dimensional excitable media.

We were able to determine the parameters of the normal form from numerical simulations of the modified Barkley model.[32,34] Using these numerically determined parameters, we showed excellent agreement between the normal form and the full partial differential equation. We quantitatively described the Hopf bifurcation and the inhomogeneous pitchfork bifurcation with the normal form. Moreover, we were able to quantify the Bogdanov–Takens bifurcation.

Whereas the subcritical character of the pitchfork bifurcation had been established in Ref. 28, a detailed analysis of the Hopf bifurcation was missing. For example, an interesting question is whether the Hopf bifurcation is subcritical (as numerically observed for the parameters chosen in Ref. 28 for the modified Barkley model), or whether it is possible to observe sustained stable oscillations. This has important implications for cardiac alternans as described above. In this paper, we will analyze the Hopf bifurcation of the normal form in detail. We derive a normal form for the Hopf bifurcation that allows us to determine the stability of the bifurcating solutions close to criticality.

Before we embark on the analytical investigation of the Hopf bifurcation and the implications for cardiac dynamics, we state that all conclusions drawn obviously depend on the validity of the normal form. So far the proposed normal form that we briefly review in Sec. II has not been rigorously derived for any excitable medium. However, we point out that in Ref. 28, we have shown good quantitative agreement with some real excitable media. We will discuss the limitations of our approach in more detail in Sec. V.

In Sec. II, we recall the normal form and some of its properties. In Sec. III, we perform a center manifold reduction of the normal form to describe the character of the Hopf bifurcation for a single pulse in a ring. In Sec. IV, we look at the case in which a pseudocontinuum of modes undergoes a Hopf bifurcation and derive in a multiple scale analysis a Ginzburg–Landau equation that allows us to study the stability of the Hopf bifurcation of a wave train. The paper concludes with Sec. V, in which we present results from numerical simulations, discuss the implications of our analysis to cardiac dynamics, and make connections to previous studies on alternans. In particular, we show that our condition for the onset of the Hopf bifurcation coincides with the well known restitution condition for cardiac alternans.

II. A NORMAL FORM

In Ref. 28, we introduced a normal form for a single pulse on a periodic domain with length L,

$$\partial_t X = -\mu - gX^2 - \beta(\gamma + X(t-\tau) + \gamma_1 X(t)), \tag{1}$$

where

$$\beta = \beta_0 \exp(-\kappa\tau) \tag{2}$$

for positive β, κ, γ, and γ_1. Here $X(t)$ may be, for example, the difference of the amplitude or the velocity of a pulse to its respective value at the saddle node. The terms proportional to β incorporate finite domain effects associated with the activator of an excitable medium running into its own inhibitor with speed c_0 after the temporal delay $\tau=(L-\nu)/c_0$, where ν is the finite width of the pulse. Note that for $\beta=0$ (i.e., for the isolated pulse with $\tau\to\infty$) we recover the generic saddle-node bifurcation, which is well known for excitable media. Numerical simulations of excitable media show that the bifurcations of a *single* propagating pulse in a ring are different from the bifurcations of a wave train consisting of several distinct pulses. In the case of a wave train with finite wavelength where a pulse may run into the inhibitor created by its preceding pulse, we showed that it was sufficient to consider two alternating populations of pulses X and Y. We derived the following extension:

$$\begin{aligned} \partial_t X &= -\mu - gX^2 - \beta(\gamma + Y(t-\tau) + \gamma_1 X(t)), \\ \partial_t Y &= -\mu - gY^2 - \beta(\gamma + X(t-\tau) + \gamma_1 Y(t)). \end{aligned} \tag{3}$$

To avoid confusion, we state that we use the term *normal form* here in two different contexts. Equations (1) and (3) are coined "normal form" as they are an attempt to describe the behavior of traveling waves in generic one-dimensional excitable media. However, these normal forms exhibit a rather rich bifurcation behavior. We will focus in Sec. III on the solution behavior close to criticality. In that context, we will speak of "normal forms" in the sense of bifurcation theory.

A. Properties of the normal form

1. Saddle-node bifurcation

Equation (1) supports the following stationary solutions:

$$\bar{X}_{1,2} = \frac{1}{2g}[-\beta(1+\gamma_1) \pm \sqrt{\beta^2(1+\gamma_1)^2 - 4g(\mu+\beta\gamma)}]. \tag{4}$$

It is readily seen that the upper solution branch is stable whereas the lower one is unstable.[28] The two solutions coalesce in a saddle-node bifurcation with

$$\bar{X}_{\mathrm{SN}} = -\frac{\beta}{2g}(1+\gamma_1) \quad \text{at} \quad \mu_{\mathrm{SN}} = \frac{\beta^2}{4g}(1+\gamma_1)^2 - \beta\gamma. \tag{5}$$

One expects the parameter β, which describes the coupling to the inhibitor, to be small (see Ref. 28). This implies $\mu_{\mathrm{SN}}<0$, indicating that the saddle node of a single pulse or of a periodic wave train on a finite ring occurs at smaller

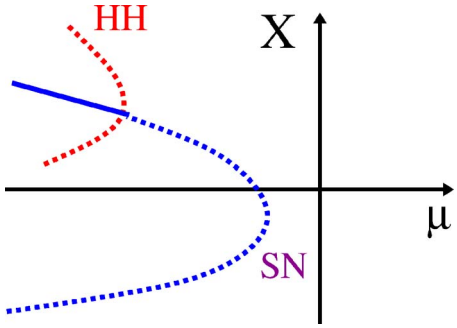

FIG. 2. (Color online) Sketch of the bifurcation diagram for a single pulse in a ring showing a stationary saddle-node bifurcation (SN) and a subcritical Hopf bifurcation (HH).

values of the bifurcation parameter μ than for the isolated pulse. Hence, the bifurcation is shifted to the left when compared to the isolated pulse (see Fig. 2).

Besides this stationary saddle-node bifurcation, the normal form equation (1) also contains a Hopf bifurcation.

2. Hopf bifurcation

Linearization of the normal form around the homogeneous solution $\bar{X}$ with respect to small perturbations of the form $\delta X \exp \lambda t$ with $\lambda=\sigma+i\omega$ yields

$$\lambda + 2g\bar{X} + \beta\gamma_1 + \beta e^{-\lambda\tau} = 0. \tag{6}$$

Besides the stationary saddle-node bifurcation equation (5) for $\lambda=0$, the linearization equation (6) also reveals the existence of a Hopf bifurcation for $\lambda=i\omega$. We readily find from Eq. (6)

$$\omega = \beta \sin \omega\tau, \tag{7}$$

$$\bar{X}_H = -\frac{\beta}{2g}(\cos \omega\tau + \gamma_1). \tag{8}$$

The first equation (7) allows us to formulate a necessary condition for the existence of a Hopf bifurcation

$$\beta\tau > 1,$$

i.e., if the coupling is strong enough and the pulse feels the presence of the inhibitor of the preceding pulse sufficiently strongly. The Hopf bifurcation occurs in parameter space before the saddle-node bifurcation and bifurcates from the upper stable branch $\bar{X}_1$ of Eq. (4) as is readily seen by observing $\bar{X}_H \geqslant \bar{X}_{\mathrm{SN}}$, independent of the value of β. Hence we may equate $\bar{X}_H=\bar{X}_1$ and solve for the bifurcation parameter. Setting $\mu_H=\mu_{SN}-\delta\mu$, we find

$$\delta\mu = \frac{\beta^2}{4g}(1-\cos \omega\tau)^2. \tag{9}$$

The saddle-node bifurcation coalesces with the Hopf bifurcation in a codimension-2 Bogdanov–Takens point. At the Bogdanov–Takens point with $\mu_H=\mu_{\mathrm{SN}}$, we have $\omega\tau=0$ and $\omega=0$, i.e., the period of the oscillation goes to infinity. The amplitude at the Bogdanov–Takens point is readily determined by comparison of Eq. (5) with Eq. (8) for $\omega\tau=0$. From Eq. (7), we infer that this occurs at $\beta\tau=1$. We note that if $\beta\tau$ is large enough, there can be arbitrary many solutions ω_l of Eq. (7). We will discuss this scenario in Sec. IV.

In Fig. 2, we show a schematic bifurcation diagram with the saddle-node bifurcation and the subcritical Hopf bifurcation for a single pulse in a ring.

3. Spatially inhomogeneous pitchfork bifurcation

When a group of several pulses in a ring is numerically simulated, one observes that this wave train group does not undergo a symmetry-preserving Hopf bifurcation on increasing the refractoriness, but instead develops a symmetry-breaking, spatially inhomogeneous instability whereby every second pulse dies.

The normal form equation (3) is able to predict and quantitatively describe this scenario.[28] The system (3) for wave trains supports two types of solutions. Besides the homogeneous solution (4), $\bar{X}_h=\bar{Y}_h=\bar{X}_1$, which may undergo a saddle-node bifurcation as described by Eq. (5), there exists another stationary solution, an alternating mode X_a and Y_a, with

$$\bar{X}_a = -\bar{Y}_a + \frac{\beta}{g}(1-\gamma_1). \tag{10}$$

Associated with this alternating solution is a pitchfork bifurcation at

$$\mu_{\mathrm{PF}} = \frac{1}{4}\frac{\beta^2(1+\gamma_1)^2}{g} - \frac{\beta^2}{g} - \beta\gamma = \mu_{\mathrm{SN}} - \frac{\beta^2}{g} \leqslant \mu_{\mathrm{SN}}, \tag{11}$$

when

$$X_{\mathrm{PF}} = Y_{\mathrm{PF}} = \frac{\beta}{2g}(1-\gamma_1). \tag{12}$$

The pitchfork bifurcation sets in before the saddle-node bifurcation as can be readily seen from Eq. (11).

The upper branch of the homogeneous solution $\bar{X}_h$ given by Eq. (4) at the pitchfork bifurcation point μ_{PF} coincides with Eq. (12). Hence as the Hopf bifurcation, the pitchfork bifurcation branches off the upper branch of the homogeneous solution. The pitchfork bifurcation is always subcritical because there are no solutions $\bar{X}_a$ possible for $\mu > \mu_{\mathrm{PF}}$. No bifurcation theory is needed to determine the subcritical character of the pitchfork bifurcation.

The stability of the homogeneous solution $\bar{X}=\bar{Y}=\bar{X}_h=\bar{Y}_h$ is determined by linearization. We study perturbations $X=\bar{X}_h+x \exp \lambda t$ and $Y=\bar{X}_h+y \exp \lambda t$, and obtain as a condition for nontrivial solutions x and y,

$$(\lambda + 2g\bar{X}_h + \beta\gamma_1) = \pm \beta e^{-\lambda\tau}. \tag{13}$$

The upper sign denotes an antisymmetric mode $x=-y$ whereas the lower sign denotes a symmetric mode $x=y$. Stationary bifurcations are characterized by $\lambda=0$, and in this case the symmetric mode coincides with the saddle-node bifurcation equation (5) and the antisymmetric mode terminates at the pitchfork bifurcation equation (12).

As for the case of a single pulse in a ring, nonstationary Hopf bifurcations are possible if $\lambda=i\omega$ for wave trains. We obtain from Eq. (13)

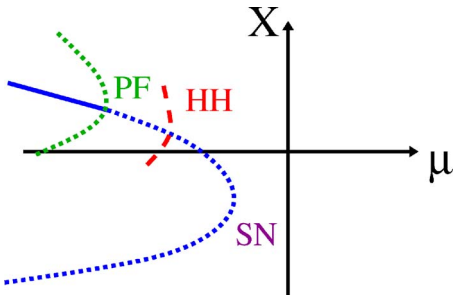

FIG. 3. (Color online) Sketch of the bifurcation diagram for a wave train in a ring showing a stationary saddle-node bifurcation (SN) and a subcritical pitchfork bifurcation (PF). In between these two bifurcations is also a Hopf bifurcation (HH).

$$\omega = \mp \beta \sin \omega\tau \tag{14}$$

and

$$\bar{X}_h = \frac{\beta}{2g}(\pm \cos \omega\tau - \gamma_1). \tag{15}$$

We consider only the symmetric case (the lower signs), which reproduces our results (7) and (8) for the symmetry-preserving Hopf bifurcation. The antisymmetric case does not allow for a single-valued positive ω. For $\omega\tau \to 0$, the onset of the Hopf bifurcation moves toward the saddle node equation (5) and coalesces with it at $\beta\tau=1$ in a Bogdanov–Takens point as described in Sec. II A. For $\omega\tau \to \pi$, the Hopf bifurcation moves toward the pitchfork bifurcation with a limiting value of $\bar{X}_h=\beta(1-\gamma_1)/(2g)=X_{\mathrm{PF}}$ in a codimension-2 bifurcation. At the point of coalescence, the Hopf bifurcation has a period $T=2\tau$, which corresponds exactly to the inhomogeneous pitchfork bifurcation with $p=\pi$ whereby every second pulse dies. For values $\omega\tau \in [0,\pi)$, the Hopf bifurcation always sets in after the pitchfork bifurcation. Hence for wave trains one can see only a Hopf bifurcation of the steady solution at the point where the Hopf bifurcation collides with the pitchfork bifurcation.

This allows us to sketch the full bifurcation scenario for a wave train in a periodic ring as depicted in Fig. 3. In the subsequent sections, we study the bifurcations of the steady-state solution (4).

III. BIFURCATION ANALYSIS OF THE HOPF BIFURCATION FOR A SINGLE PULSE

In this section, we study the direction and the stability of the Hopf bifurcation. In excitable media, the Hopf bifurcation is a result of stronger and stronger coupling of the activator with its own inhibitor. Upon reducing the length of a ring for fixed excitability, or reducing the excitability for a fixed ring length, a single pulse will feel the tail of its own inhibitor created during its previous passage through the ring. In a wave train, each pulse will feel the tail of the inhibitor of its neighbor in front. In the context of our normal form equation (1), the increasing coupling translates into an increase of $\beta\tau$. Upon increasing $\beta\tau$ from $\beta\tau=1$ up to a critical value of $\beta\tau \approx 7.789$, we have only one solution $\omega=\omega_0$ of the characteristic equation (7); see Fig. 6. We will study now the dynamics for this case. The case of arbitrary many solutions when one encounters a pseudocontinuum of frequencies will be discussed in Sec. IV.

The theory of bifurcation analysis for delay-differential equations is well developed.[35–38] For example, in Ref. 38, a formula for the coefficients of the normal form for a Hopf bifurcation is given explicitly. However, we found that the theory of delay differential equations is not as well known among scientists as its age may suggest. We find it instructive, therefore, to perform the calculations explicitly and lead the reader through the calculations.

To study the direction of the Hopf bifurcation, we have to determine the sign of $d\sigma/d\mu$ at the bifurcation point μ_H. From Eq. (6), we infer

$$\frac{d\lambda}{d\mu} = -\frac{2g}{1-\beta\tau e^{-\lambda\tau}}\frac{d\bar{X}}{d\mu}.$$

Using Eq. (9), we find from Eq. (4)

$$\left.\frac{d\bar{X}}{d\mu}\right|_{\mu_H} = -\frac{1}{\beta(1-\cos\omega\tau)},$$

and subsequently

$$\left.\frac{d\sigma}{d\mu}\right|_{\mu_H} = \frac{2g}{\beta}\frac{1}{\|1-\beta\tau e^{-\lambda\tau}\|} > 0, \tag{16}$$

which implies that the stationary solution loses stability with increasing values of the bifurcation parameter μ.

We now study the character of the Hopf bifurcation and derive the normal form for a Hopf bifurcation from Eq. (1). In order to do that, we first transform the normal form equation (1) into standard form by subtracting the stationary solution (4) according to $X=\bar{X}+x$, where $\bar{X}=\bar{X}_1$. We obtain

$$\partial_t x = -2g\bar{X}x - \beta(x(t-\tau)+\gamma_1 x(t)) - gx^2, \tag{17}$$

with the stationary solution being now $x(t)=0$. We will employ a center manifold reduction for this equation to describe the dynamics close to criticality. Center manifold theory is well-established for maps, ordinary differential equations, and partial differential equations. However, although known for some time,[35–37] it is not well known how to formulate an essentially infinite-dimensional delay differential equation such as Eq. (1) into a form such that center manifold reduction can be applied. For ordinary differential equations, for example, the application of center manifold theory is a straightforward expansion of the state vectors in critical eigenmodes. The problem for delay differential equations is their inherent infinite-dimensional character. An initial condition $x(\theta)=x_0(\theta)$ for $-\tau \leqslant \theta \leqslant 0$ is mapped onto a finite-dimensional space, in the case of Eq. (17), onto a one-dimensional space. Lacking uniqueness of solutions is one obstacle that prohibits a straightforward application of center manifold reduction. The trick with this dilemma is to reformulate the problem as a *mapping* from an infinite-dimensional space of differentiable functions defined on the interval $[-\tau,0]$, which we denote as $\mathcal{C}=\mathcal{C}[[-\tau,0];\mathbb{R}]$ [i.e., $x_0(\theta) \in \mathcal{C}$], onto itself. This allows us to employ the well established and understood center manifold reduction for

mappings. These ideas go back to Hale.[36,35] We found well written examples of center manifold reductions to be examined in Refs. 39–41. In essence, the history of a state vector $x(t)\in\mathbb{R}$ is folded to a single element of an extended state space $x_t(\theta)\in\mathcal{C}$. In order to achieve this, we define $x_t(\theta)\in\mathcal{C}$ as

$$x_t(\theta)=x(t+\theta) \quad \text{for } -\tau\leqslant\theta\leqslant 0.$$

The time evolution for $x(t)\in\mathbb{R}$ [Eq. (17)] needs to be reexpressed in terms of propagators and operators acting on elements of the extended state space $x_t(\theta)\in\mathcal{C}$, which can be done by writing

$$\frac{d}{dt}x_t(\theta)=\mathcal{A}[x_t](\theta)=\begin{cases}\dfrac{d}{d\theta}x_t(\theta) & \text{if } -\tau\leqslant\theta<0\\ \mathcal{F}[x_t] & \text{if } \theta=0\end{cases}. \tag{18}$$

For $-\tau\leqslant\theta<0$, we used the invariance condition $dx(t+\theta)/dt=dx(t+\theta)/d\theta$. For $\theta=0$, we can split the operator $\mathcal{F}$ into a linear part $\mathcal{L}$ and a nonlinear part $\mathcal{N}$ and reformulate the right-hand side of Eq. (17) as

$$\mathcal{F}[x_t]=\mathcal{L}[x_t]+\mathcal{N}[x_t], \tag{19}$$

where

$$\mathcal{L}[x_t]=\int_{-\tau}^{0}d\theta w_1(\theta)x_t(\theta)$$
$$\text{with } w_1(\theta)=-(2g\bar{X}+\beta\gamma_1)\delta(\theta)-\beta\delta(\theta+\tau) \tag{20}$$

and

$$\mathcal{N}[x_t]=\int_{-\tau}^{0}d\theta_1 d\theta_2 w_2(\theta_1,\theta_2)x_t(\theta_1)x_t(\theta_2)$$
$$\text{with } w_2(\theta_1,\theta_2)=-g\delta(\theta_1)\delta(\theta_2), \tag{21}$$

where $\delta(\theta)$ denotes the Dirac δ function. Once $x_t(\theta)$ is computed via solving Eq. (18), one may convert back to $x(t)$ by

$$x(t)=\int_{-\tau}^{0}d\theta\delta(\theta)x_t(\theta).$$

A. Linear eigenvalue problem

We now linearize Eq. (18) around the stationary solution $x_t(\theta)=0$ to obtain

$$\frac{d}{dt}\xi_t(\theta)=\mathcal{A}_L[\xi_t](\theta)=\begin{cases}\dfrac{d}{d\theta}\xi_t(\theta) & \text{if } -\tau\leqslant\theta<0\\ \mathcal{L}[\xi_t] & \text{if } \theta=0\end{cases}. \tag{22}$$

The linear eigenvalue problem (22) can be solved using the ansatz

$$\xi_t(\theta)=e^{\lambda t}\Phi(\theta) \quad \text{for } -\tau\leqslant\theta\leqslant 0.$$

On the interval $-\tau\leqslant\theta<0$, we obtain

$$\lambda\Phi(\theta)=\frac{d}{d\theta}\Phi(\theta),$$

which is solved by

$$\Phi(\theta)=e^{\lambda\theta}\Phi(0). \tag{23}$$

Plugging the solution (23) into Eq. (22), we can now evaluate the $\theta=0$ part of Eq. (22) to obtain again the characteristic equation (6). We recall the transcendental characteristic equation as

$$\lambda+2g\bar{X}+\beta\gamma_1+\beta e^{-\lambda\tau}=0. \tag{24}$$

Since in general the linear operator $\mathcal{A}_L$ is not self-adjoint, we need to consider the corresponding adjoint eigenvalue problem on the dual extended state space $\mathcal{C}^\dagger=\mathcal{C}^\dagger[[0,\tau];\mathbb{R}]$. The dual problem is given by backward evolution for $t\leqslant 0$, i.e., $x_t^\dagger(s)=x_{-t}(-s)$ for $0\leqslant s\leqslant\tau$. The adjoint problem can be formally written as

$$\frac{d}{dt}\xi_t^\dagger(s)=-\mathcal{A}_L^\dagger[\xi_t](s).$$

To provide an explicit form of the dual operator $\mathcal{A}_L$, we need to define an inner product. It turns out that the normal scalar product used for ordinary differential equations is not capable of respecting the memory effects of delay-differential equations. The following inner product is used:

$$\langle\Psi^\dagger,\Phi\rangle=\Psi^\dagger(0)\Phi(0)-\int_{-\tau}^{0}d\theta\int_{0}^{\theta}ds\Psi^\dagger(s-\theta)w_1(\theta)\Phi(s). \tag{25}$$

The adjoint operator is then explicitly given as

$$\mathcal{A}_L^\dagger[\xi_t](s)=\begin{cases}-\dfrac{d}{ds}\xi_t^\dagger(s) & \text{if } 0<s\leqslant\tau\\ \mathcal{L}^\dagger[\xi_t^\dagger] & \text{if } s=0\end{cases}, \tag{26}$$

where

$$\mathcal{L}^\dagger[\xi_t^\dagger]=\int_{0}^{\tau}dsw_1(-s)\xi_t^\dagger(s). \tag{27}$$

The adjoint eigenvalue problem (26) is now solved using the ansatz

$$\xi_t^\dagger(s)=e^{-\lambda t}\Psi^\dagger(s) \quad \text{for } 0<s\leqslant\tau.$$

On the interval $0<s\leqslant\tau$, we obtain

$$-\lambda\Psi^\dagger(s)=\frac{d}{ds}\Psi^\dagger(s),$$

which is solved by

$$\Psi^\dagger(s)=e^{-\lambda s}\Psi^\dagger(0). \tag{28}$$

Plugging the solution (28) into Eq. (27), we can now evaluate the $s=0$ part of Eq. (26) to obtain again the characteristic equation (24). Note that the two solutions (23) and (28) for the eigenvalue problem and its dual can be transformed into each other by simple time reversal $\theta\to -s$.

Since the transcendental equation has two solutions with vanishing real part $\sigma=0$, i.e., $\lambda=\pm i\omega$ with ω given by Eq.

(7), we have two solutions of the linear eigenvalue problem (22) and its associated adjoint problem (26). We denote them as $\Phi_{1,2}$ and $\Psi^{\dagger}_{1,2}$, respectively. The bilinear form (25) was constructed in order to assure biorthogonality of the eigenfunctions. Defining the eigenfunctions as

$$\Phi_1(\theta) = e^{i\omega\theta}, \quad \Phi_2(\theta) = e^{-i\omega\theta}, \tag{29}$$

$$\Psi^{\dagger}_1(s) = \nu e^{-i\omega s}, \quad \Psi^{\dagger}_2(s) = \nu^{\star} e^{i\omega s} \tag{30}$$

with the normalization constant

$$\nu = \frac{1}{1 - \beta\tau e^{-i\omega\tau}}, \tag{31}$$

we have $\langle \Psi^{\dagger}_i, \Phi_j \rangle = \delta_{ij}$ with $i,j=1,2$ and δ_{ij} being the Kronecker symbol.

B. Center-manifold theory

For the nonlinear theory, we need properties for the linear operator $\mathcal{A}$ developed in Refs. 36 and 37. We summarize properties of the transcendental characteristic equation (6): (i) $\mathcal{A}$ has a pure point spectrum, (ii) the real part of the eigenvalues is bounded from above, and (iii) defining $a=\tau\{2g\bar{X}+\beta\gamma_1\}$ and $b=\beta\tau$, all eigenvalues of $\mathcal{A}$ have negative real part if and only if (1) $a>-1$, (2) $a+b>0$, and (3) $b<\zeta \sin\zeta - a\cos\zeta$, where ζ is the root of $\zeta=-a\tan\zeta$ with $0<\zeta<\pi$ for $a\neq 0$ and $\zeta=\pi/2$ if $a=0$. These conditions can be translated for our particular case (24) using $a=-\beta\tau\cos(\omega\tau)$. Condition (1) translates into $\beta\tau\cos(\omega\tau)<1$, condition (2) into $\cos(\omega\tau)<1$, and condition (3) defines a parametrized stability boundary $\beta\tau<\zeta/\sin(\zeta)$ and $\cos(\omega\tau)>\cos(\zeta)$ with $0<\zeta<\pi$. This last condition defines the line in $\beta\tau$-$\cos(\omega\tau)$ space where the Hopf bifurcation occurs. In particular, we have $\beta\tau\geqslant 1$ and a coalescence with the saddle node at $\cos(\omega\tau)=1$ with $\beta\tau=1$ at the Bogdanov–Takens point. In Fig. 4, we show the stability region. We note that care has to be taken in interpreting the diagram in terms of the parameter τ because $\beta=\beta(\tau)$ according to Eq. (2). In the limit $\tau\to\infty$, we have $\beta\tau\to 0$. Note that stable solutions may exist for $\beta\tau\geqslant 1$.

In Refs. 36 and 37, it was shown that under these circumstances, one may perform center manifold reduction. In particular, we can decompose $x_t(\theta)$ into slow modes associated with the eigenvalues $\lambda=\pm i\omega$ and fast modes which correspond to modes with negative real part of the eigenvalues. Center manifold theory says that the fast modes are slaved to the slow modes and can be expressed in terms of the slow modes. We therefore write

$$x_t(\theta) = z(t)\Phi_1(\theta) + z^{\star}(t)\Phi_2(\theta) + h(z,z^{\star}), \tag{32}$$

where $z(t)\in\mathbb{C}$ and its complex conjugate $z^{\star}(t)$ are the time-dependent amplitudes of the slow modes $\Phi_{1,2}(\theta)$ and $h(z,z^{\star})$ is the remaining fast component written as a function of the slow amplitudes. The function $h(z,z^{\star})$ is called the center manifold. The expansion (32) resembles the center-manifold theory for partial differential equations where θ would be the spatial coordinate, and the expansion would be an expansion of critical spatial eigenmodes. The connection between delay differential equations and partial differential equations will be explored further in Sec. IV.

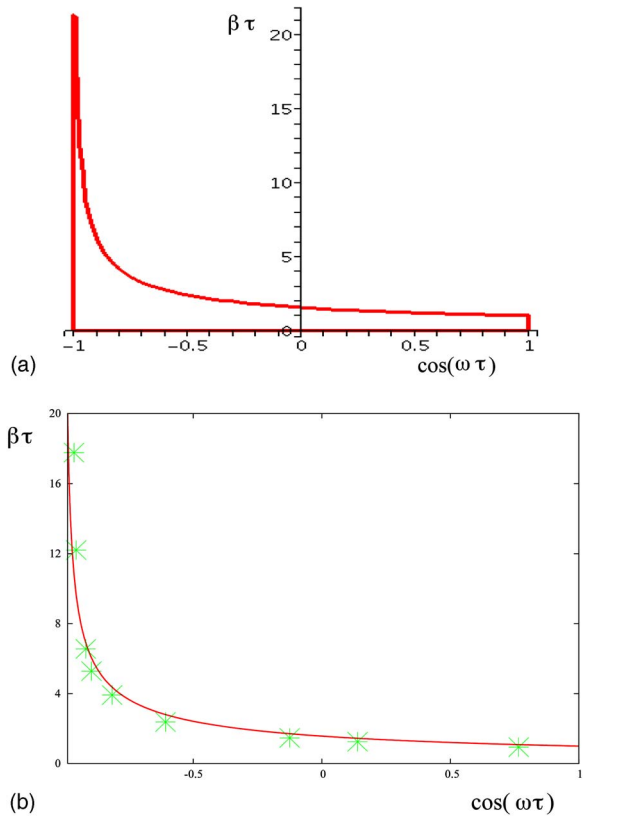

FIG. 4. (Color online) (a) Stability diagram for the equilibrium solution (4). We also impose $\beta\tau\geqslant 0$. The region within the bold lines is stable. Crossing the upper boundary corresponds to a Hopf bifurcation. (b) Hopf line obtained by numerical simulations of the modified Barkley model (70) with $a=0.22$ and $u_s=0.1$ and $D=3$ (Refs. 32 and 34). (Note that each point corresponds to different values of ϵ and L.) The numerical results of the partial differential equations could be fitted to the normal form equation (1) to obtain the parameters β_0 and τ, see Ref. 28. The continuous line is the same Hopf line as in (a).

We require the fast modes, and hence the center manifold, to lie in the spectral complement of the center space spanned by $\Phi(\theta)$; we therefore have the constraint

$$\langle \Psi^{\dagger}_j, h(z,z^{\star}) \rangle = 0 \quad j=1,2.$$

This implies for the slow amplitudes

$$z(t) = \langle \Psi^{\dagger}_1(\theta), x_t(\theta) \rangle \quad \text{and} \quad z^{\star}(t) = \langle \Psi^{\dagger}_2(\theta), x_t(\theta) \rangle. \tag{33}$$

We use a near-identity transformation for the center manifold h and express it as a power series in z and $z^{\star}$. The center manifold is tangential to the manifold spanned by the slow modes, which implies the ansatz

$$h(z,z^{\star}) = \tfrac{1}{2}(h_{20}(\theta)z^2 + 2h_{11}(\theta)zz^{\star} + h_{02}(\theta)z^{\star 2}) + \mathcal{O}(|z|^3). \tag{34}$$

Since $x_t(\theta)$ is real, we have $h_{02}(\theta)=h^{\star}_{20}(\theta)$. Since the normal form for a Hopf bifurcation only involves cubic terms, we only need to consider quadratic terms in the equation for h [Eq. (37)]. The cubic terms will then be generated via $\mathcal{N}[x_t](\theta=0)$ in the equations for z and $z^{\star}$ [see below, Eqs. (35) and (36)].

We will derive now ordinary differential equations for the slow amplitudes z and $z^\star$, which describe the dynamics on the slow manifold. The theory of center manifolds tells us that the full dynamics of Eq. (17) is well approximated by the slow dynamics.[42] The derivative of Eq. (33) with respect to time t is given by

$$\begin{aligned}\dot{z} &= \langle \Psi_1^\dagger, \dot{x}_t\rangle = i\omega\langle \Psi_1^\dagger, x_t\rangle + \langle \Psi_1^\dagger, \mathcal{N}[x_t]\rangle|_{\theta=0} \\ &= i\omega z + \Psi_1^\dagger(0)\mathcal{N}[x_t](\theta=0) = i\omega z + \nu\mathcal{N}[x_t](\theta=0), \quad (35)\end{aligned}$$

$$\dot{z}^\star = -i\omega z^\star + \nu^\star \mathcal{N}[x_t](\theta=0), \quad (36)$$

$$\begin{aligned}\dot{h} &= \dot{x}_t - \dot{z}\Phi_1(\theta) - \dot{z}^\star\Phi_2(\theta) \\ &= \mathcal{A}_L x_t + \mathcal{N}[x_t] - i\omega z\Phi_1(\theta) + i\omega z^\star\Phi_2(\theta) - \mathcal{N}[x_t](\theta=0) \\ &\quad \times\{\nu\Phi_1(\theta) + \nu^\star\Phi_2(\theta)\} \\ &= \mathcal{A}_L h + \mathcal{N}[x_t] - \{\nu\Phi_1(\theta) + \nu^\star\Phi_2(\theta)\}\mathcal{N}[x_t](\theta=0), \quad (37)\end{aligned}$$

where the dot denotes a time derivative. Note that $\mathcal{N}[x_t]\neq 0$ only for $\theta=0$, which can be written as $\mathcal{N}[x_t](\theta=0)=\mathcal{N}[z\Phi_1+z^\star\Phi_2+h(z,z^\star)](\theta=0)$. Using Eq. (34), we have therefore

$$\begin{aligned}\mathcal{N}[x_t](\theta=0) &= -g x_t^2(\theta=0) \\ &= -g(z\Phi_1 + z^\star\Phi_2 + h)^2|_{\theta=0} \\ &= -g(z^2 + z^{\star 2} + 2|z|^2 + h_{20}(0)z^3 \\ &\quad + (h_{20}(0) + 2h_{11}(0))|z|^2 z \\ &\quad + (h_{02}(0) + 2h_{11}(0))|z|^2 z^\star + h_{02}(0)z^{\star 3}) \\ &\quad + \mathcal{O}(z^4, z^{\star 4}). \quad (38)\end{aligned}$$

Using the definition of $\mathcal{A}_L$ and $\mathcal{N}[x_t]$, we can evaluate the evolution equation (18) by differentiating the center manifold equation (34) with respect to time, equate with Eq. (37), and obtain

$$\begin{aligned}\dot{h} &= i\omega h_{20}(\theta)z^2 - i\omega h_{02}(\theta)z^{\star 2} \\ &= -2\mathcal{R}[\nu e^{i\omega\theta}]\mathcal{N}[x_t](\theta=0) \\ &\quad + \begin{cases} \dfrac{d}{d\theta}h(\theta) & \text{if } -\tau \leqslant \theta < 0 \\ \mathcal{H}[z,z^\star;h] & \text{if } \theta = 0 \end{cases}, \quad (39)\end{aligned}$$

where

$$\mathcal{H}[z,z^\star;h] = -(2g\bar{X} + \beta\gamma_1)h(0) - \beta h(-\tau) + \mathcal{N}[x_t](\theta=0). \quad (40)$$

Here $\mathcal{R}$ denotes the real part.

Comparison of powers of z and $z^\star$ yields differential equations for h_{ij} for the part with $-\tau\leqslant\theta<0$ with an associated boundary value problem coming from a comparison of powers of z and $z^\star$ from the $\theta=0$ part. We summarize

$$h_{20}' = 2i\omega h_{20} - 4g\mathcal{R}[\nu e^{i\omega\theta}], \quad (41)$$

$$h_{02}' = -2i\omega h_{02} - 4g\mathcal{R}[\nu e^{i\omega\theta}], \quad (42)$$

$$h_{11}' = -4g\mathcal{R}[\nu^{i\omega\theta}], \quad (43)$$

and the boundary conditions are given by

$$(i\omega - \beta e^{-i\omega\tau})h_{20}(0) + \beta h_{20}(-\tau) = 2g(2\mathcal{R}[\nu] - 1), \quad (44)$$

$$(-i\omega - \beta e^{i\omega\tau})h_{02}(0) + \beta h_{02}(-\tau) = 2g(2\mathcal{R}[\nu] - 1), \quad (45)$$

$$(-i\omega - \beta e^{-i\omega\tau})h_{11}(0) + \beta h_{11}(-\tau) = 2g(2\mathcal{R}[\nu] - 1). \quad (46)$$

Note that the nonlinearity enters the differential equation in the form of an inhomogeneity. The ordinary differential equations (41)–(43) can be solved by variations of constants

$$h_{20}(\theta) = H_{20}e^{2i\omega\theta} - 2i\frac{g}{\omega}\left(\nu e^{i\omega\theta} + \frac{1}{3}\nu^\star e^{-i\omega\theta}\right), \quad (47)$$

$$h_{02}(\theta) = H_{02}e^{-2i\omega\theta} + 2i\frac{g}{\omega}\left(\nu^\star e^{-i\omega\theta} + \frac{1}{3}\nu e^{i\omega\theta}\right), \quad (48)$$

$$h_{11}(\theta) = H_{11} + 2i\frac{g}{\omega}(\nu e^{i\omega\theta} - \nu^\star e^{-i\omega\theta}). \quad (49)$$

The constants of integrations $H_{20}=H_{02}^\star$ and H_{11} can be determined using the boundary conditions (44)–(46). We obtain

$$H_{20} = -\frac{2g}{i\omega - \beta e^{-i\omega\tau} + \beta e^{-2i\omega\tau}}, \quad (50)$$

$$H_{11} = -\frac{2g}{-i\omega - \beta e^{-i\omega\tau} + \beta}. \quad (51)$$

Note that $H_{11}=-2g/(\beta-\beta\cos(\omega\tau))=H_{11}^\star$. By means of transformations,[43] Eq. (35) can be transformed into the standard form for a normal form for Hopf bifurcations,

$$\dot{z} = i\omega z + c|z|^2 z. \quad (52)$$

The quadratic terms appearing in Eq. (35) can be eliminated by the near-identity transformation $z\to z+\eta_{20}z^2+\eta_{11}|z|^2+\eta_{02}z^{\star 2}$ using $\eta_{20}=ig\nu/\omega$, $\eta_{11}=-2ig\nu/\omega$, and $\eta_{02}=-ig\nu/3\omega$. Note that at the Bogdanov–Takens point where $\omega=0$, such an elimination of quadratic terms is not possible anymore. However, this transformation generates further cubic terms in Eq. (35). All of these cubic terms except those proportional to $|z|^2z$ may be eliminated by means of another transformation $z\to z+h_3(z,z^\star)$, where $h_3(z,z^\star)$ is a cubic polynomial. After the transformation to eliminate the quadratic terms, the coefficient in front of the $|z|^2z$ term is found to be

$$\begin{aligned}c &= -g\nu(h_{20}(0) + 2h_{11}(0)) + (2\eta_{02}g\nu^\star + 2\eta_{11}g\nu^\star \\ &\quad - \eta_{11}(i\omega\eta_{20} + 3g\nu) - 2\eta_{20}(2i\omega\eta_{11} - g\nu) - 2\eta_{02}g\nu) \\ &= -g\nu(h_{20}(0) + 2h_{11}(0)) - \frac{14}{3}ig^2\frac{|\nu|^2}{\omega} + \frac{20}{3}ig^2\frac{\nu^2}{\omega} \\ &= -g\nu(H_{20} + 2H_{11}) + \frac{14}{3}ig^2\frac{\nu^2}{\omega}. \quad (53)\end{aligned}$$

The stability and character of the Hopf bifurcation are determined by the sign of the real part of c. Because of Eq. (16), the Hopf bifurcation is supercritical provided $\mathcal{R}[c]<0$ and

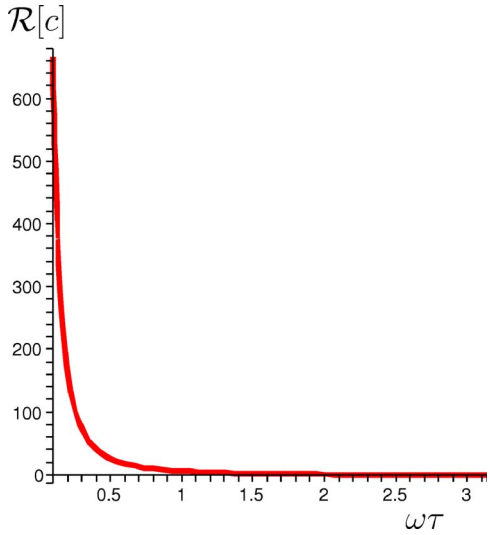

FIG. 5. (Color online) Plot of the real part of the cubic coefficient $\mathcal{R}[c]$ [Eq. (53)] as a function of $\omega\tau$. To produce the plot, we set $g=1$ and $\tau=1$. Both parameters are just coefficients multiplying c, so they do not change the sign of c.

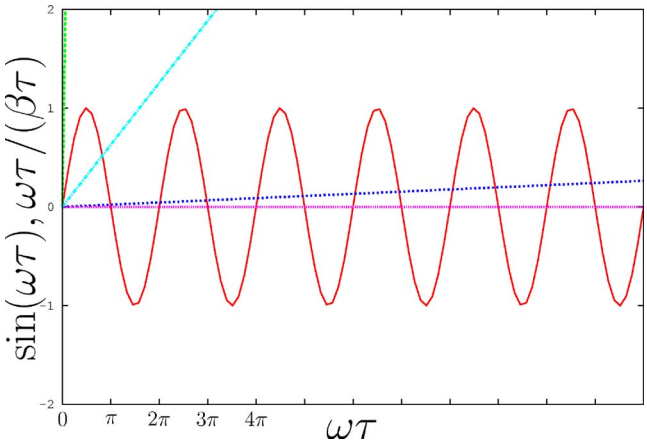

FIG. 6. (Color online) Illustration of the solutions and number of solutions of the implicit equation (54) for ω. Green curve: $\beta\tau=0.1$, no Hopf bifurcation; light blue curve: $\beta\tau=5$, Hopf bifurcation with one marginal mode; dark blue curve: $\beta\tau=143$, Hopf bifurcation with finitely many marginal modes; pink curve: $\beta\tau=\infty$, Hopf bifurcation with infinitely many marginal modes.

subcritical provided $\mathcal{R}[c]>0$. These criteria can be easily deduced by writing $z=re^{i\phi}$. Note that $\mathcal{R}[c]$ can be written as a function of g, τ, and ω only since $\beta=\omega/\sin(\omega\tau)$ at the Hopf bifurcation. Using algebraic software packages such as MAPLE, we can show that $\mathcal{R}[c]>0$ for all values of g, τ, and β. In Fig. 5, we show the real part of c as a function of $\omega\tau$. This confirms that the Hopf bifurcation is indeed subcritical, as conjectured in Ref. 28. We have checked our result against numerical simulations of the full normal-form equation (1) and also using the software package DDE-BIFTOOL.[44] Again, the degeneracy at $\omega\tau\to 0$ is reflected in $\mathcal{R}[c]$ by a singularity at $\omega\tau=0$.

We will discuss the implications of this result in Sec. V.

IV. THE LIMIT OF LARGE DELAY TIMES: THE HOPF BIFURCATION FOR WAVE TRAINS

In the preceding section, we described the Hopf bifurcation for small $\omega\tau$ when there is only one marginal mode. This describes the behavior of a single pulse on a ring. In this section, we will pursue the case of large delay times when a pseudocontinuum of critical Hopf modes occurs. We will derive a Ginzburg–Landau equation as an amplitude equation describing near-threshold behavior of such a pseudocontinuum. The connection between amplitude equations and delay-differential equations has long been known.[45–50] The crossover from a finite-dimensional center manifold to an infinite-dimensional amplitude equation can be best viewed when looking at the Hopf condition (7),

$$\omega = \beta \sin \omega\tau. \tag{54}$$

For $\beta\tau>7.789$, there are at least two solutions of Eq. (54) for ω. This equation has arbitrary many solutions ω_k for $\beta\tau\to\infty$ and we obtain a pseudocontinuum in an interval with lower closed boundary at $\omega\tau$ and upper boundary $\omega\tau=\pi$. At the singular limit $\omega\tau=\pi$, there are countably infinitely many eigenvalues $\omega_k\tau=k\pi$. An illustration is given in Fig. 6. Note that the upper boundary $\omega\tau=\pi$ corresponds to the coalescence of the Hopf bifurcation with the pitchfork bifurcation in the case of several pulses on a ring (see Sec. II).

All these solutions are marginal and would have to be included in the ansatz (32). Note that for excitable media where $\beta=\beta_0\exp(-\kappa\tau)$ [see Eq. (2)], this limit cannot be achieved by simply letting $\tau\to\infty$. The function $\beta\tau$ has a maximum at $\tau=1/\kappa$. So in order to have $\beta\tau\to\infty$, one can either have $\beta_0\to\infty$, which seems unphysical, or $\kappa\to 0$ with $\tau\to\infty$ to keep $\kappa\tau$ finite. Hence the limit $\beta\tau\to\infty$ applies to media with a very slowly decaying inhibitor in a very large domain. Large domain instabilities are known from certain excitable reaction diffusion systems in the context of autocatalytic oxidation of CO to CO_2 on platinum.[51–53]

The case $\omega\tau\approx\pi$ is important for single pulses in a ring and for wave trains. Firstly, it describes the case for a single pulse when a continuum of modes becomes unstable to a Hopf bifurcation. But more importantly, it describes the case of a wave train with distinct members when the pitchfork bifurcation coalesces with the Hopf bifurcation. The point of coalescence is at μ_{PF} given by Eq. (11) and with amplitude given by Eq. (12) which we recall,

$$X_{\mathrm{PF}} = \frac{\beta}{2g}(1-\gamma_1).$$

At this point of coalescence, the Hopf frequency is in resonance with the spatial instability in which every second pulse dies. At μ_{PF}, the two equations (3) describing the alternating modes in a wave train collapse to the single equation for one pulse (1) (see also Fig. 3). This section will investigate whether the coalescence of the subcritical pitchfork bifurcation with the Hopf bifurcation may produce stable oscillations.

We will perform a multiple scale analysis of the normal form equation (1) along the lines of Ref. 48. We will obtain at third order an evolution equation for the amplitude as a solvability condition that describes the dynamics close to the Hopf bifurcation. We consider the case of large delay times τ

and introduce a small parameter $\epsilon=1/\tau$. To capture the dynamics close to the point of coalescence, we introduce a slow time scale

$$s=\epsilon t,$$

and rewrite the normal form equation (1) in terms of the slow variable as

$$\epsilon\partial_s X=-\mu-gX^2-\beta(\gamma+X(s-1)+\gamma_1 X). \tag{55}$$

We expand the scalar field $X(s)$ as

$$X=x_{\mathrm{PF}}+\epsilon x_1+\epsilon^2 x_2+\epsilon^3 x_3+\cdots .$$

Using the generic scaling, the bifurcation parameter can be written as

$$\mu=\mu_{\mathrm{PF}}+\epsilon^2\Delta\mu+\cdots .$$

A Taylor expansion of Eq. (54) around $\omega\tau=\pi$ yields at first order $\omega\tau=\beta\tau(\pi-\omega\tau)$, which for large τ (small ϵ) we may write as

$$\omega\tau=\pi\left(1-\frac{1}{\beta\tau}+\frac{1}{(\beta\tau)^2}\right)=\pi\left(1-\frac{1}{\beta}\epsilon+\frac{1}{\beta^2}\epsilon^2\right). \tag{56}$$

This suggests a multiple time scaling

$$\partial_s=\partial_{s_0}+\epsilon\partial_{s_1}+\epsilon^2\partial_{s_2}+\cdots .$$

Close to the bifurcation point, critical slowing down occurs that allows us to expand the delay term for large delays as

$$X(s-1)=e^{-\partial_s}X(s), \tag{57}$$

$$\approx\left[1-\epsilon\partial_{s_1}+\epsilon^2\left(\tfrac{1}{2}\partial_{s_1s_1}-\partial_{s_2}\right)\right]e^{-\partial_{s_0}}X(s). \tag{58}$$

At lowest order, $\mathcal{O}(1)$, we obtain the equation determining x_{PF}. At the next order, we obtain

$$\mathcal{L}x_1=0, \tag{59}$$

with the linear operator

$$\mathcal{L}=\beta[1+e^{-\partial_{s_0}}].$$

Equation (59) is solved by

$$x_1(s_0,s_1,s_2)=z(s_1,s_2)e^{i\pi s_0}+\bar{z}(s_1,s_2)e^{-i\pi s_0}, \tag{60}$$

with complex amplitude z and its complex conjugate $\bar{z}$. Note that on the fast time scale t we would have $x_1(t)=z\exp(i\omega t)+$c.c. with $\omega\tau=\pi$, which, of course, is the Hopf mode at onset.

At the next order, $\mathcal{O}(\epsilon^2)$, we obtain

$$\mathcal{L}x_2=-\Delta\mu-gx_1^2-\partial_{s_0}x_1+\beta\partial_{s_1}e^{-\partial_{s_0}}x_1. \tag{61}$$

The right-hand side involves terms proportional to $\exp(\pm i\pi s_0)$, which are resonant with the homogeneous solution of $\mathcal{L}x_2=0$. We therefore impose the solvability condition

$$\partial_{s_0}x_1-\beta\partial_{s_1}e^{-\partial_{s_0}}x_1=0,$$

which, using Eq. (59), reads

$$\partial_{s_1}x_1+\frac{1}{\beta}\partial_{s_0}x_1=0. \tag{62}$$

In terms of the complex amplitude z using Eq. (60), this reads

$$\partial_{s_1}z+\frac{1}{\beta}i\pi z=0. \tag{63}$$

This amounts to the time scale $i\omega\tau\approx\tau\partial_t\approx\partial_{s_0}+\epsilon\partial_{s_1}=i\pi-i\epsilon\pi/\beta=i\pi(1-1/(\beta\tau))$, which corresponds to our scaling equation (56) at first order. Provided Eq. (63) is satisfied, we can readily solve Eq. (61) by solving for each appearing harmonic, and find

$$\begin{aligned}x_2&=-\frac{1}{2\beta}[\Delta\mu+2g|z|^2+gz^2e^{2i\pi s_0}+g\bar{z}^2e^{-2i\pi s_0}]\\&=-\frac{1}{2\beta}[\Delta\mu+gx_1^2],\end{aligned} \tag{64}$$

where we used Eq. (59).

At the next order, $\mathcal{O}(\epsilon^3)$, we obtain the desired evolution equation as a solvability condition. At $\mathcal{O}(\epsilon^3)$, we obtain

$$\begin{aligned}\mathcal{L}x_3&=-\partial_{s_0}x_2+\beta\partial_{s_1}e^{-\partial_{s_0}}x_2-\partial_{s_1}x_1-2gx_1x_2\\&\quad-\tfrac{1}{2}\beta\partial_{s_1s_1}e^{-\partial_{s_0}}x_1+\beta\partial_{s_2}e^{-\partial_{s_0}}x_1\\&=-\partial_{s_0}x_2+\beta\partial_{s_1}e^{-\partial_{s_0}}x_2-\partial_{s_1}x_1-2gx_1x_2+\tfrac{1}{2}\beta\partial_{s_1s_1}x_1\\&\quad-\beta\partial_{s_2}x_1.\end{aligned} \tag{65}$$

Again resonant terms proportional to $\exp(\pm i\pi s_0)$ are eliminated by imposing a solvability condition that, upon using the expressions for x_2, yields the desired amplitude equation,

$$\partial_{s_2}x_1-\frac{1}{\beta^2}\partial_{s_0}x_1=\frac{g}{\beta^2}\Delta\mu x_1+\frac{1}{2\beta^2}\partial_{s_0s_0}x_1+\frac{g^2}{\beta^2}x_1^3. \tag{66}$$

This is the well-studied real Ginzburg–Landau equation.[54] The time-like variable is the slow time scale s_2 and the space-like variable the faster time scale s_0, which is $\mathcal{O}(\tau)$. As in the finite-dimensional case studied in Sec. III, the Hopf bifurcation is clearly subcritical since the real part of the coefficient in front of the cubic term in Eq. (66) is positive for all parameter values. Hence the coalescence of the Hopf bifurcation and the pitchfork bifurcation cannot lead to stable oscillations. We have shown that wave trains also undergo unstable oscillations in the framework of the normal form equation (1).

The usefulness of the spatiotemporal viewpoint for delay differential equations as expressed here in the Ginzburg–Landau equation (66) has been pointed out.[45,46,48,50] However, the Ginzburg–Landau equation (66) may be cast into a finite-dimensional system that emphasizes the underlying multiple scale analysis. We start by rewriting Eq. (66) as an equation for the complex amplitude z. One can explicitly express s_0-derivatives and obtain the following finite-dimensional system:

$$\partial_{s_2} z - i\pi \frac{1}{\beta^2} z = \frac{g}{\beta^2}\left(\Delta\mu - \frac{\pi^2}{2g}\right) z + 3\frac{g^2}{\beta^2}|z|^2 z. \tag{67}$$

The time-scaling on the left-hand side is as expected from our initial linearization and expansion of the frequency equation (56). We have in total

$$i\omega\tau \approx \tau\partial_t = \partial_s \approx \partial_{s_0} + \epsilon\partial_{s_1} + \epsilon^2\partial_{s_2} = i\pi\left(1 - \frac{1}{\beta\tau} + \frac{1}{(\beta\tau)^2}\right),$$

which corresponds to Eq. (56). This illustrates the multiple-scale character of our analysis where the nonlinear term may be interpreted as a frequency correction.[55] The correction term to the linear term on the right-hand side of Eq. (67) shows that the onset is retarded on the very slow time scale s_2.

In Ref. 21, a real Ginzburg–Landau equation was derived for paced excitable media with an additional integral term modeling the pacing. It would be interesting to see whether the amplitude equation derived therein can be derived in a multiple scale analysis along the lines of this multiple scale analysis.

V. SUMMARY AND DISCUSSION

We have explored the Hopf bifurcations of a single pulse and of a wave train in a ring of excitable medium. We have found that for the phenomenological normal form equation (1), the Hopf bifurcation for a single pulse on a ring and for a wave train on a ring is always subcritical independent of the equation parameters.

Hopf bifurcations in excitable media had been previously studied. Besides numerical investigations of the Barkley model,[33] the modified Barkley model,[34] the Beeler–Reuter model,[56,57,11,29,30,58] the Noble model,[59,17,29] and the Karma model,[17] where a Hopf bifurcation has been reported, there have been many theoretical attempts to quantify this bifurcation for a single pulse on a ring. Interest has risen recently in the Hopf bifurcation in the context of cardiac dynamics because it is believed to be a precursor of propagation failure of pulses on a ring. The Hopf bifurcation has been related to a phenomenon in cardiac excitable media that goes under the name of *alternans*. Alternans describe the scenario whereby action potential durations are alternating periodically between short and long periods. The interest in alternans has risen as they are believed to trigger spiral wave breakup in cardiac tissue and ventricular fibrillation.[11,15–18]

Our results may shed new light on what may be called *alternans*. The occurrence of alternans in clinical situations is often followed by spiral wave breakup and ventricular fibrillation.[11,15–18] The subcritical character of the Hopf bifurcation gives a simple and straightforward explanation for this phenomenon. Moreover, if the system length L is slowly varied, long transients may be observed of apparently stable oscillations (see Figs. 7 and 8). Depending on whether the system length is below or above the critical length L_H, the oscillations will relax toward the homogeneous state or the instability will lead to wave breakup. However, even for the case of relaxation toward the stable homogeneous solution, these oscillations may lead to wave breakup upon further reduction of the system length, because of the subcritical character of the Hopf bifurcations. This illustrates the diagnostic importance of cardiac alternans.

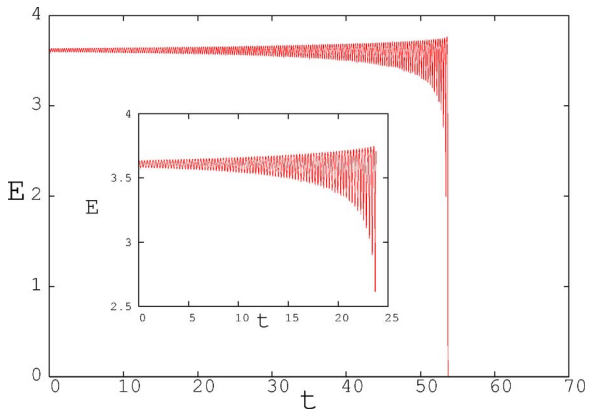

FIG. 7. (Color online) Temporal behavior of the maximal amplitude $E_{\max}$ of the activator E for model (69) just above the subcritical Hopf bifurcation. The parameters are $A=1.5415$, $\epsilon=0.009$, $M=30$, $n_B=0.525$, and $L=0.215$. The inset shows the behavior at $L=0.210$.

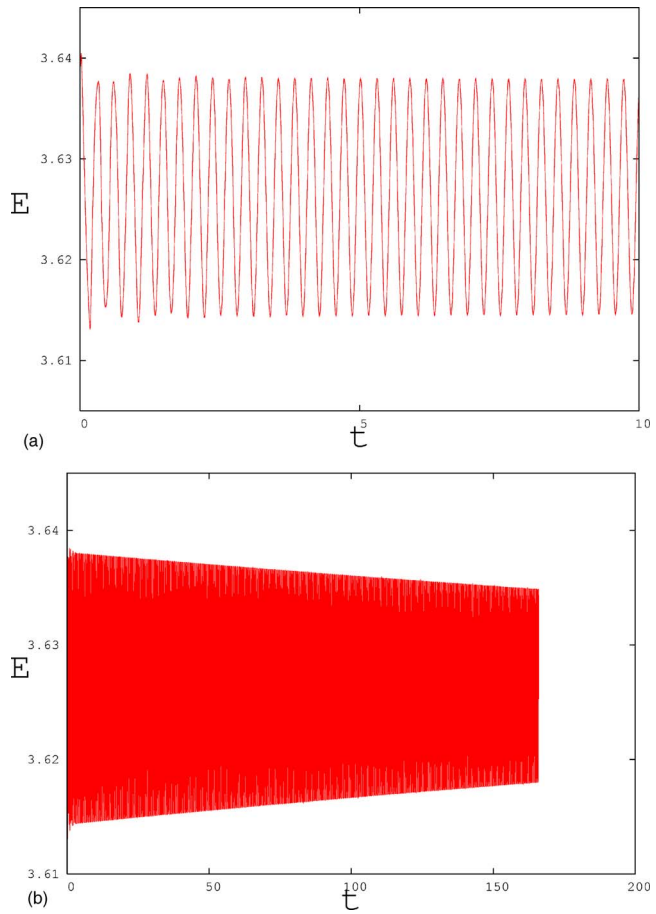

FIG. 8. (Color online) Temporal behavior of the maximal amplitude $E_{\max}$ of the activator E for model (69). The system length is just below the Hopf bifurcation with $L=0.22$; the other parameters are as in Fig. 7. (a) The oscillations appear to be stable over some time. (b) Same parameters as in (a) but longer integration time. The apparent stability has to be accounted for by insufficiently long integration times. The solution adjusts to the homogeneous solution. Note the long time scales which contain hundreds of oscillations.

A. Limitations and range of validity of our results

Strictly speaking, our result that the Hopf bifurcation is subcritical for the normal form equation (1) cannot be taken as proof that alternans are unstable for all excitable media. The normal form equation (1) is only valid for a certain class of excitable media. In particular, it describes the situation in which an activator weakly interacts with the inhibitor of the preceding exponentially decaying inhibitor. Moreover, the normal form has only been phenomenologically derived in Ref. 28. Of course, unless a rigorous derivation of the normal form equation (1) has been provided, the results presented here may serve as nothing more than a guidance in interpreting alternans in real cardiac systems or more complex ionic models of excitable media, and may alert scientists to check results on stability of oscillations more carefully.

Several simplifications have been made to obtain the normal form equation (1) in Ref. 28. For example, the time delay $\tau=L/c_0$ is treated as constant. This is obviously not correct for Hopf bifurcations. However, the inclusion of γ_1 (which is essential in the quantitative description of the Hopf bifurcation) allows for velocity-dependent effects. Guided by the success of the normal form to quantitatively describe a certain class of excitable media and by numerical experiments, we are hopeful that our result may help to interpret experiments and numerical simulations.

In Sec. V C, we will discuss a particular model for cardiac dynamics in which for certain parameter values the assumptions for the derivation of our normal form are violated. For these parameter values, stable oscillations may occur. However, even for systems that are described by the normal form equation (1), a word of caution is appropriate. If the oscillatory solutions bifurcating from the stationary solution are unstable as we have proven here, the unstable Hopf branch could in principle fold back and restabilize. Our analysis does not include such secondary bifurcations. Another scenario that we cannot exclude based on our analysis is that the unstable branch may be a basin of attraction for a stable oscillatory solution far away from the homogeneous solution. However, our numerical simulations do not hint toward such scenarios.

From an observational perspective, the relevance of the subcritical instability for spiral wave breakup is a matter of the time scale of the instability. The time scale associated with the subcritical Hopf bifurcation may be very long, as seen in Fig. 9. This time scale becomes shorter the further the perturbation in the bifurcation parameter is from its value at the corresponding stable stationary pulse solution. In any case, if the parameter is kept fixed above the critical value, the instability will eventually develop unless the lifetime of a reentrant spiral is less than the time scale of the instability. For clinical applications, one would need to estimate the time scale of a reentrant spiral and compare it with the time scale of the instability. Such estimates, however, are not meaningful for simple models such as the Barkley model.

Our definition of alternans is restricted to nonpaced pulses on a ring. If the excitable media is paced, the subcritical character of the Hopf bifurcation is not guaranteed anymore, and there is no *a priori* reason why stable alternans cannot occur. Indeed, in periodically stimulated excitable media, stable alternans have been reported.[60,61,19–21,23,24] A nonpaced single pulse on a ring is a simple model for a reentrant spiral moving around an anatomical obstacle or around a region of partially or totally inexcitable tissue. As such, it ignores the dynamics of the spiral away from the obstacle. An extension would be to look at a transversal one-dimensional slice through a spiral and consider wave trains and instabilities of such wave trains.

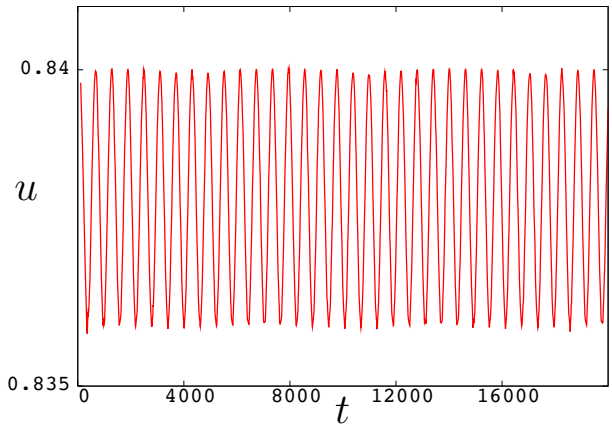

FIG. 9. (Color online) Temporal behavior of the maximal amplitude $u_{\max}$ of the activator u for model (70) just above the subcritical Hopf bifurcation. The parameters are $a=0.22$, $u_s=0.1$, $\epsilon=0.03755$, and $L=246$. The oscillations appear stable for a very long time but will eventually either damp out and attain a constant nonzero value in the case in which L is larger than the critical L_H at which the Hopf bifurcation occurs, or in the case $L<L_H$ the pulse will collapse as depicted in Fig. 7, confirming the subcritical character of the Hopf bifurcation.

B. Relation to the restitution condition

Since the pioneering work of Ref. 12, alternans have been related to a period-doubling bifurcation. This work has rediscovered the results from Ref. 15, which had hardly been noticed by the scientific community until then. Therein, it was proposed that the bifurcation can be described by a one-dimensional return map relating the action potential duration (APD) to the previous recovery time, or diastolic interval (DI), which is the time between the end of a pulse to the next excitation. A period-doubling bifurcation was found if the slope of the so called restitution curve, which relates the APD to the DI, exceeds 1. A critical account on the predictive nature of the restitution curve for period-doubling bifurcations is given in Refs. 62 and 23. In Ref. 29, the instability was analyzed by reducing the partial differential equation describing the excitable media to a discrete map via a reduction to a free-boundary problem. In Ref. 34, the Hopf bifurcation could be described by means of a reduced set of ordinary-differential equations using a collective coordinate approach. In Refs. 11, 30, 58, and 26, the bifurcation was linked to an instability of a single integro-delay equation. The condition for instability given by this approach states—as in some previous studies involving one-dimensional return maps—that the slope of the restitution curve needs to be greater than 1. However, as evidenced in experiments[63,64] and in theoretical studies,[62,23,65–67] alternans do not necessarily occur when the slope of the restitution

curve is greater than 1. In our work, we have a different criterion for alternans (which we interpret now as unstable periodic oscillations). Our necessary condition for the occurrence of alternans, $\beta\tau>1$, does not involve the restitution curve but involves the coupling strength and the wavelength. Moreover, in Fig. 4(b) we can see that for our normal form, pulses can be stable for values of $\beta\tau\gg 1$ in accordance with the above-mentioned experiments and numerical studies.

In the following, we will show how our necessary condition for the onset of instability $\beta\tau>1$ can be related to the restitution condition that the onset of instability is given when the slope of the restitution curve exceeds 1.

Close to the saddle node, the Hopf frequency is $\omega\tau\approx 0$. We introduce a small parameter $\delta\ll 1$ and write close to the saddle node,

$$X=\bar{X}_{\mathrm{SN}}+\delta x,$$

where $\bar{X}_{\mathrm{SN}}$ is given by Eq. (5). The generic scaling close to the saddle node implies that we may write $\mu=\mu_{\mathrm{SN}}+\delta^2\Delta\mu$. Using the critical slowing down at the saddle node and the fact that $\omega\tau\approx 0$, we may approximate the normal form equation (1) to describe the temporal change of X at some time t and at some later time $t+\tau$:

$$\frac{\delta x_{n+1}-\delta x_n}{\tau}=-\mu_{\mathrm{SN}}-\delta^2\Delta\mu-g(\bar{X}_{\mathrm{SN}}+\delta x_n)^2 - \beta(\gamma+\bar{X}_{SN}+\gamma_1\bar{X}_{\mathrm{SN}}+\delta x_{n-1}+\gamma_1\delta x_n).$$

Here $x_n=x(t_n)$ and $x_{n+1}=x(t_n+\tau)$. Neglecting terms of $\mathcal{O}(\delta^2)$ and using the definition of the saddle node equation (5), we end up with

$$x_{n+1}-(1+\beta\tau)x_n+\beta\tau x_{n-1}=0.$$

This equation has either the solution $x_n=1$, which corresponds to the stable steady solution described by $\bar{X}_1$ of Eq. (4), or

$$x_n=(\beta\tau)^n x_0,$$

which implies the "map"

$$x_n=\beta\tau x_{n-1}. \tag{68}$$

Close to the saddle node, the amplitude of the activator x_n correlates well with the APD, and we find that $\beta\tau>1$ is exactly the restitution condition whereby the slope of the restitution curve has to be larger than 1.

Our model contains the restitution condition as a limiting case when the Hopf bifurcation occurs close to the saddle node. However, as seen in Fig. 4, $\beta\tau$ may be larger than 1 but still the system supports stable pulses. These corrections to the restitution conditions are captured by our model. Moreover, the normal form is able to determine the frequency at onset.

We note that the parameter γ_1 does not enter the restitution condition; it is not needed for the *existence* of a Hopf bifurcation [cf. Eqs. (7) and (8)]. However, as pointed out in Ref. 28, quantitative agreement with numerical simulations is only given if γ_1 is included. In Ref. 28, the inclusion of the γ_1 term takes into account the velocity-dependent modifications of the bifurcation behavior: large-amplitude pulses have a higher velocity than low-amplitude ones. A larger pulse will therefore run further into the inhibitor generated by its predecessor. Velocity restitution curves have been studied in Ref. 65 to allow for a modification of the restitution condition derived in Ref. 30 for a single pulse in a ring. The normal form incorporates naturally these velocity-dependent terms.

For a recent numerical study on the validity of the restitution condition, the reader is referred to Ref. 67. In this work, the stability of certain excitable media is investigated by means of numerical continuation methods, which allow a precise identification of the onset of oscillations. At the onset of alternans, the restitution curve was determined. It was found that the restitution condition failed for three out of four cases for pulses in a one-dimensional ring. Our result suggests that the restitution condition may be a good indicator for the onset of alternans close to the saddle node.

C. Numerical simulations

In the context of alternans, the Hopf bifurcation had been described as a supercritical bifurcation[11,17,29,30] and not, as we have found here, as a subcritical bifurcation (although at the same time their occurrence had been related to wave breakup[29]). We therefore revisit some of the previous numerical studies. In Ref. 17, the following two-variable model was proposed:

$$\epsilon\partial_t E=\epsilon^2\partial_{xx}E-E+\left[A-\left(\frac{n}{n_B}\right)^M\right](1-\tanh(E-3))\frac{E^2}{2}, \tag{69}$$

$$\partial_t n=\theta(E-1)-n,$$

as a model for action potential propagation in cardiac tissue. Here $\theta(x)$ is the Heaviside step function. This model incorporates essential features of electrophysiological cardiac models. For the parameters $A=1.5415$, $\epsilon=0.009$, $M=30$, and $n_B=0.525$, a supercritical Hopf bifurcation was reported upon diminishing the system length L. We integrate this model using a pseudospectral Crank–Nicholson method where the nonlinearity is treated with an Adams–Bashforth scheme. We use a time step of $dt=0.00001$ and 4096 spatial grid points. A Hopf bifurcation occurs around $L=0.215$. To approach the Hopf bifurcation, we created a stable pulse for some large system length, and subsequently diminished the system length L. In Fig. 7, we show that for these parameters the bifurcation is actually subcritical. The subcritical character has not been recognized before—probably because of insufficiently short integration times. For system length L just above the critical length, the oscillations can appear stable for a very long time (see Fig. 8) before they settle down to the homogeneous solution.

Indeed, as already stated in our paper,[28] the number of oscillations may be rather large when the instability is weak. In Fig. 9, we show such a case for the maximal amplitude of the activator u for the modified Barkley model,

$$\partial_t u = D\partial_{xx} u + u(1-u)(u-u_s-v),$$
$$\partial_t v = \epsilon(u-av), \tag{70}$$

which is a reparametrized version of a model introduced by Barkley.[32] It is clearly seen that the oscillations can appear stable for a very long time and many oscillations (in this case, more than 500 oscillations), which has led scientists to the false conclusion that the Hopf bifurcation is supercritical.

The normal forms Eq. (1) or Eq. (3) were derived for situations in which the activator weakly interacts with the tail of the preceding inhibitor which exponentially decays toward the homogeneous rest state. Then one can describe the influence of the tail of the preceding inhibitor as a perturbation to the generic saddle node of the isolated pulse. The models discussed so far all fall into this category. A different model was introduced by Echebarria and Karma in Ref. 21, which, as we will see below, for certain parameter regions does not fall into this class of model but supports stable oscillations. Originally, the model was studied for a paced strand but recently has also been studied in a ring geometry.[68] It has been argued in Ref. 68 in the framework of amplitude equations that the nature of the bifurcation for the ring dynamics, whether supercritical or subcritical, is determined by the action potential duration restitution curve for a propagated pulse. In the following, we study numerically the Hopf bifurcation for this model in a ring geometry. This will illustrate the range of validity for our normal form and the conclusions that may be drawn with respect to the stability of cardiac alternans. The model consists of the standard cable equation,

$$\partial_t V = D\partial_{xx} V - \frac{I_{\text{ion}}}{C_m}, \tag{71}$$

where I_{ion} models the membrane current and C_m is the capacity of the membrane. In Ref. 21, the following form for the membrane current was proposed:

$$\frac{I_{\text{ion}}}{C_m} = \frac{1}{\tau_0}\left(S + (1-S)\frac{V}{V_c}\right) - \frac{1}{\tau_a}hS, \tag{72}$$

with a switch function

$$S = \frac{1}{2}\left(1 + \tanh\left(\frac{V-V_c}{\epsilon}\right)\right). \tag{73}$$

The gate variable h evolves according to

$$\frac{dh}{dt} = \frac{1-S-h}{\tau_m(1-S)+\tau_p S}. \tag{74}$$

The stable homogeneous rest state is at $V=0$ and $h=1$; however, for small τ_a a second stable focus may arise. For details on the physiological interpretations of the model, the reader is referred to Refs. 21 and 68. For the numerical integration, we use again a semi-implicit pseudospectral Crank–Nicholson method where the nonlinearity is treated with an Adams–Bashforth scheme. We use a time step of $dt=0.01$ and 1024 spatial grid points. In Fig. 10, we show an example for a subcritical Hopf bifurcation in this model consistent with our theory. However, for sufficiently small τ_a a supercritical Hopf bifurcation arises upon decreasing the ring length L. In Fig. 11, we present a space-time plot for such a situation of stable oscillations. Whereas the subcritical case is consistent with our theory, we now have to understand why for small τ_a, stable oscillations occur. In order to do so, it is helpful to look at the spatial profiles of the activator and the inhibitor close to the Hopf bifurcation, which are presented in Fig. 12. In Fig. 12(a), we see the activator V and the inhibitor $1-h$ for the case of a subcritical Hopf bifurcation as seen in Fig. 10. The figure is similar to Fig. 1 for the modified Barkley model. The activator weakly interacts with the exponentially decaying tail of the inhibitor it created during its previous revolution. In this parameter region, our normal form is valid and correctly predicts a subcritical bifurcation. In Fig. 12(b), the situation is depicted for the supercritical case seen in Fig. 11. Here the situation is very different. The inhibitor does not approach the homogeneous rest state $1-h=0$ but rather develops a metastable $1-h=1$ plateau. This has two consequences: first, the solution is driven away from the homoclinic pulse solution around which the normal form is built, and second, the interaction is not weak anymore. The reason for this different behavior can be understood by looking at the nullclines of the homoge-

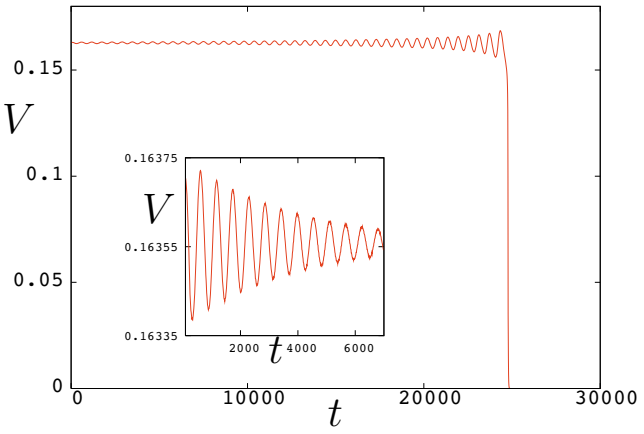

FIG. 10. (Color online) Temporal behavior of the maximal amplitude $V_{\max}$ of the activator V for model (71)–(74). The parameters are $\tau_0=150$, $\tau_a=26$, $\tau_m=60$, $\tau_p=12$, $V_c=0.1$, $D=0.00025$, and $\epsilon=0.005$. The main figure is obtained for $L=1.11$, which is slightly above the subcritical Hopf bifurcation confirming the subcritical character of the Hopf bifurcation. The inset is for $L=1.1175$, which is slightly below the bifurcation point.

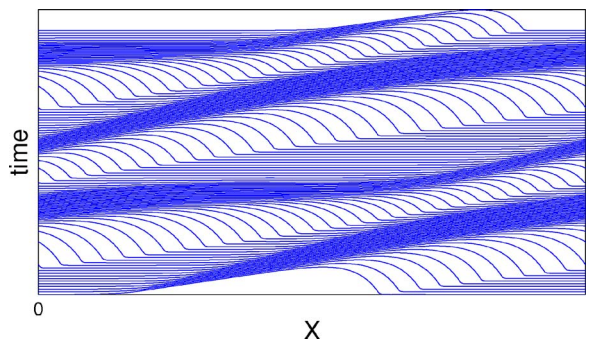

FIG. 11. (Color online) Space-time plot of stable oscillations occurring at $\tau_a=6$ with $L=4.8$ for the model (71)–(74). The other parameters are as in Fig. 10. Stable oscillations are found for a range of ring lengths L.

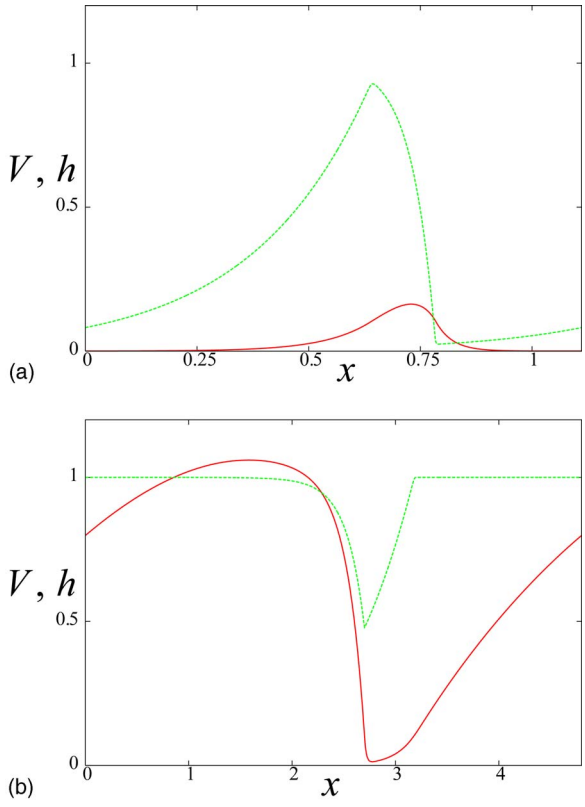

FIG. 12. (Color online) Plot of the activator V (continuous line) and the inhibitor h (dashed line) for the system (71)–(74). We plot here $1-h$ rather than h to have the homogeneous rest state at $u=0$ and $1-h=0$. Parameters are $\tau_0=150$, $\tau_m=60$, $\tau_p=12$, $V_c=0.1$, $D=0.00025$, and $\epsilon=0.005$. (a) The activator runs into the exponentially decaying tail of the inhibitor, which decays toward the rest state $1-h=0$. This is similar to the behavior in Fig. 1. Parameters are $\tau_a=26$ with $L=1.11$. This scenario is well described by the normal form. (b) The activator does not interact with the exponentially decaying tail corresponding to the rest state but rather with the metastable state defined by $\dot{h}=0$. Parameters are $\tau_a=6$ with $L=4.8$. This case cannot be captured by the normal form.

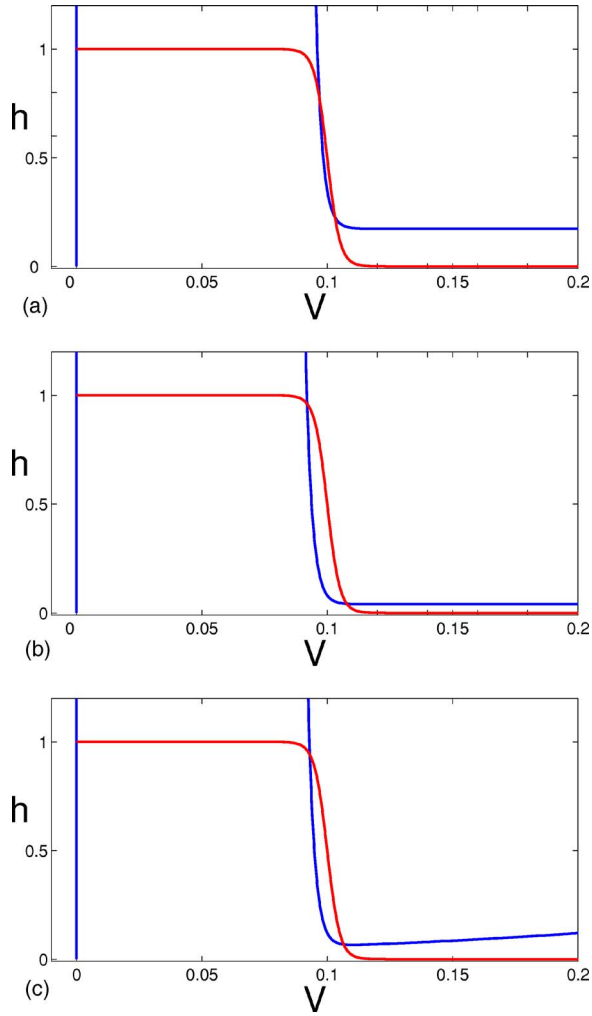

FIG. 13. (Color online) Nullclines for the system (71)–(74). The darker lines denote the $\dot{V}=0$ nullclines and the lighter lines the $\dot{h}=0$ nullclines. Parameters are $\tau_0=150$, $\tau_m=60$, $\tau_p=12$, $V_c=0.1$, and $\epsilon=0.005$, and for all cases only one stable fixed point exists at $V=0$ and $h=1$. (a) The subcritical case with $\tau_a=26$. (b) The supercritical case with $\tau_a=6$. Note the closeness of the nullclines for large V. (c) Nullclines for the modified equation (75) which breaks the near degeneracy of the nullclines observed in (b). Here $\tau_a=6$ and $\tau_l=3$.

neous problem of Eqs. (71)–(74), i.e., by setting $\partial_x=0$. In Fig. 13, we show the nullclines for the two cases $\tau_a=6$ (supercritical) and $\tau_a=26$ (subcritical). Note that for $\tau_a=6$, the only stable fixed point is at $V=0$ and $h=1$. The difference is that in the supercritical case the $\dot{h}=0$ nullcline and the $\dot{V}=0$ nullcline are very close to each other. This forces the trajectory to spend a long time on the $\dot{h}=0$-nullcline near $h=0$ (as seen in the plateau part of the spatial profile of $1-h=1$ in Fig. 11). We call this state a metastable state. For decreasing ring length, it dominates the profile of the inhibitor and does not allow the inhibitor to come close to the rest state $h=1$. Therefore, our normal form, which is formulated around the saddle-node of the pulse, breaks down. The solution is not close to the traveling pulse in phase space anymore and our local analysis around the saddle node of the traveling wave cannot work anymore. However, we note that the system (71)–(74) is rather unusual with the two nullclines being parallel to each other with the possibility of a metastable state, resulting in rather particular dynamical behavior.

We may modify the model (71)–(74) to break the degenerate situation in which the two nullclines of the inhibitor and activator run parallel to each other and subsequently may get too close to each other for certain parameters. We can destroy the existence of the metastable state for finite ring length by allowing the nullcline of the activator to bend away from the nullcline of the inhibitor if we, for example, consider the following modification of the membrane current:

$$\frac{I_{\text{ion}}}{C_m}=\frac{1}{\tau_0}\left(S+(1-S)\frac{V}{V_c}\right)+\frac{1}{\tau_l}V^2-\frac{1}{\tau_a}hS, \tag{75}$$

with some sufficiently small τ_l. Then we are again in the situation where the rest state $V=0$ and $h=1$ dominates the dynamics upon decreasing the ring length L. The nullclines are shown in Fig. 13. We confirmed that for $\tau_l=3$, the Hopf bifurcation is indeed subcritical, consistent with our theoretical result. We note that the actual value of τ_l is not important for the existence of subcritical bifurcation but rather that a sufficiently small τ_l breaks the geometric structure of the degenerate nullclines and allows the activator nullcline to

bend away from the inhibitor nullcline. The model (71)–(74) illustrates for which class of excitable media our normal form is applicable and for which systems we may draw conclusions on the stability of dynamical alternans in a ring.

ACKNOWLEDGMENTS

I would like to thank Sebastian Hermann for helping with the DDE-BIFTOOL software, and Martin Wechselberger for fruitful discussions. I gratefully acknowledge support by the Australian Research Council, Grant Nos. DP0452147 and DP0667065.

[1]A. T. Winfree, *When Time Breaks Down* (Princeton University Press, Princeton, NJ, 1987).
[2]J. M. Davidenko, A. M. Pertsov, R. Salomonsz, W. Baxter, and J. Jalife, "Stationary and drifting spiral waves of excitation in isolated cardiac muscle," Nature (London) **335**, 349 (1992).
[3]F. Siegert and C. Weijer, "Analysis of optical density wave propagation and cell movement in the cellular slime mold dictyostelium discoideum," Physica D **49**, 224 (1991).
[4]M. D. Berridge, P. Lipp, and M. J. Bootman, "The versatility and universality of calcium signalling," Nat. Rev. Mol. Cell Biol. **1**, 11 (2000).
[5]A. T. Winfree, "Spiral waves of chemical activity," Science **175**, 634 (1972).
[6]A. T. Winfree, "Stable particle-like solutions to the nonlinear wave equations of the three-dimensional excitable media," SIAM Rev. **32**, 1 (1990).
[7]A. T. Winfree, "Electrical turbulence in three-dimensional heart muscle," Science **266**, 1003 (1994).
[8]D. Margerit and D. Barkley, "Selection of twisted scroll waves in three-dimensional excitable media," Phys. Rev. Lett. **86**, 175 (2001).
[9]D. Margerit and D. Barkley, "Cookbook asymptotics for spiral and scroll waves in excitable media," Chaos **12**, 636 (2002).
[10]See review articles in the focus issue Chaos **8** (1) (1998).
[11]M. Courtemanche, L. Glass, and J. P. Keener, "Instabilities of a propagating pulse in a ring of excitable media," Phys. Rev. Lett. **70**, 2182 (1993).
[12]M. R. Guevara, G. Ward, A. Shrier, and L. Glass, "Electrical alternans and period-doubling bifurcations," in *IEEE Computers in Cardiology* (IEEE Computer Society, Silver Spring, MD, 1984), pp. 167–170.
[13]G. R. Mines, "On circulating excitations in heart muscles and their possible relation to tachycardia and fibrillation," Trans R. Soc. Can. **4**, 43 (1914).
[14]L. H. Frame and M. B. Simson, "Oscillations of conduction, action potential duration, and refractoriness," Circulation **78**, 1277 (1988).
[15]J. B. Nolasco and R. W. Dahlen, "A graphic method for the study of alternation in cardiac action potentials," J. Appl. Physiol. **25**, 191 (1968).
[16]A. Karma, "Electrical alternans and spiral wave breakup in cardiac tissue," Chaos **4**, 461 (1994).
[17]A. Karma, "Spiral breakup in model equations of action potential propagation in cardiac tissue," Phys. Rev. Lett. **71**, 1103 (1993).
[18]F. H. Fenton, E. M. Cherry, H. M. Hastings, and S. J. Evans, "Multiple mechanisms of spiral wave breakup in a model of cardiac electrical activity," Chaos **12**, 852 (2002).
[19]H. M. Hastings, F. H. Fenton, S. J. Evans, O. Hotomaroglu, J. Geetha, K. Gittelson, J. Nilson, and A. Garfinkel, "Alternans and the onset of ventricular fibrillation," Phys. Rev. E **62**, 4043 (2000).
[20]H. Arce, A. López, and M. R. Guevara, "Triggered alternans in an ionic model of ischemic cardiac ventricular muscle," Chaos **12**, 807 (2002).
[21]B. Echebarria and A. Karma, "Instability and spatiotemporal dynamics of alternans in paced cardiac dynamics," Phys. Rev. Lett. **88**, 208101 (2002).
[22]B. Echebarria and A. Karma, "Spatiotemporal control of cardiac alternans," Chaos **12**, 923 (2002).
[23]J. J. Fox, E. Bodenschatz, and R. F. Gilmour, "Period-doubling instability and memory in cardiac tissue," Phys. Rev. Lett. **89**, 138101 (2002).
[24]H. Henry and W.-J. Rappel, "Dynamics of conduction blocks in a model of paced cardiac tissue," Phys. Rev. E **71**, 051911 (2005).
[25]A. Vinet, "Memory and bistability in a one-dimensional loop of model cardiac cells," J. Biol. Syst. **7**, 451 (1999).
[26]P. Comtois and A. Vinet, "Stability and bifurcation in an integral-delay model of cardiac reentry including spatial coupling in repolarization," Phys. Rev. E **68**, 051903 (2003).
[27]P. Comtois and A. Vinet, "Multistability of reentrant rhythms in an ionic model of a two-dimensional annulus of cardiac tissue," Phys. Rev. E **72**, 051927 (2005).
[28]G. A. Gottwald and L. Kramer, "A normal form for excitable media," Chaos **16**, 013122 (2006).
[29]A. Karma, H. Levine, and X. Zou, "Theory of pulse instabilities in electrophysiological models of excitable tissues," Physica D **73**, 113 (1994).
[30]M. Courtemanche, L. Glass, and J. P. Keener, "A delay equation representation of pulse circulation on a ring in excitable media," SIAM J. Appl. Math. **56**, 119 (1996).
[31]R. FitzHugh, "Impulses and physiological states in theoretical models of nerve membranes," Biophys. J. **1**, 445 (1961); J. Nagumo, S. Arimoto, and S. Yoshizawa, "An active pulse transmission line simulating 1214-nerve axons," Proc. IRE **50**, 2061 (1962).
[32]D. Barkley, "A model for fast computer simulation of waves in excitable media," Physica D **49**, 61 (1991).
[33]M. Knees, L. S. Tuckerman, and D. Barkley, "Symmetry-breaking bifurcations in one-dimensional excitable media," Phys. Rev. A **46**, 5054 (1992).
[34]G. A. Gottwald and L. Kramer, "On propagation failure in 1 and 2 dimensional excitable media," Chaos **14**, 855 (2004).
[35]N. Krasovskii, *Stability of Motion* (Stanford University Press, Stanford, CA, 1963).
[36]J. K. Hale, *Theory of Functional Differential Equations* (Springer-Verlag, New York, 1977).
[37]J. K. Hale and S. M. Verduyn Lunel, *Introduction to Functional Differential Equations* (Springer-Verlag, New York, 1993).
[38]O. Diekmann, S. A. van Gils, S. M. Verduyn Lunel, and H. O. Walther, *Delay Equations*, Applied Mathematics and Sciences (Springer-Verlag, New York, 1995), Vol. 110.
[39]W. Wischert, A. Wunderlin, A. Pelster, M. Olivier, and J. Groslambert, "Delay-induced instabilities in nonlinear feedback systems," Phys. Rev. E **49**, 203 (1994).
[40]B. F. Redmond, V. G. LeBlanc, and A. Longtin, "Bifurcation analysis of a class of first-order nonlinear delay-differential equations with reflectional symmetry," Physica D **166**, 131 (2002).
[41]J. Sieber and B. Krauskopf, "Bifurcation analysis of an inverted pendulum with delayed feedback control near a triple-zero eigenvalue singularity," Nonlinearity **17**, 85 (2004).
[42]J. Carr, *Application of the Center Manifold Theory*, Applied Mathematics and Sciences (Springer-Verlag, Berlin, 1981), Vol. 35.
[43]S. Wiggins, *Introduction to Applied Nonlinear Dynamical Systems and Chaos* (Springer-Verlag, New York, 1990).
[44]K. Engelborghs, T. Luzyanina, and G. Samaey, "DDE-BIFTOOL v. 2.00 user manual: A Matlab package for bifurcation analysis of delay differential equations," Technical Report TW-330, Department of Computer Science, K. U. Leuven, Leuven, Belgium (2001).
[45]G. Giacomelli and A. Politi, "Relationship between delayed and spatially extended dynamical systems," Phys. Rev. Lett. **76**, 2686 (1996).
[46]G. Giacomelli and A. Politi, "Multiple scale analysis of delayed dynamical systems," Physica D **117**, 26 (1998).
[47]M. Schanz and A. Pelster, "Analytical and numerical investigations of the phase-locked loop with time delay," Phys. Rev. E **67**, 056205 (2003).
[48]M. Nizette, "Front dynamics in a delayed-feedback system with external forcing," Physica D **183**, 220 (2003).
[49]A. Amann, E. Schöll, and W. Just, "Some basic remarks on eigenmode expansions of time-delay dynamics," Physica A **373**, 191 (2006).
[50]M. Wolfrum and S. Yanchuk, "Eckhaus instability in systems with large delay," Phys. Rev. Lett. **96**, 220201 (2006).
[51]M. G. Zimmermann, S. O. Firle, M. A. Natiello, M. Hildebrand, M. Eiswirth, M. Bär, A. K. Bangia, and I. G. Kevrekidis, "Pulse bifurcation and transition to spatiotemporal chaos in an excitable reaction-diffusion model," Physica D **110**, 92 (1997).
[52]J. Krishnan, I. G. Kevrekidis, M. Or-Guil, M. G. Zimmermann, and M. Bär, "Numerical bifurcation and stability analysis of solitary pulses in an excitable reaction-diffusion model," Comput. Methods Appl. Mech. Eng. **170**, 253 (1999).
[53]M. Or-Guil, J. Krishnan, I. G. Kevrekidis, and M. Bär, "Pulse bifurcations and instabilities in an excitable medium: Computations in finite ring domains," Phys. Rev. E **64**, 046212 (2001).
[54]I. S. Aranson and L. Kramer, "The world of the complex Ginzburg–Landau equation," Rev. Mod. Phys. **74**, 99 (2002).
[55]F. Verhulst, *Nonlinear Differential Equations and Dynamical Systems* (Springer-Verlag, New York, 2000).
[56]G. W. Beeler and H. Reuter, "Reconstruction of the action potential of ventricular myocardial fibers," J. Physiol. (London) **268**, 177 (1977).

[57]W. Quan and Y. Rudy, "Unidirectional block and reentry of cardiac excitation: A model study," Circ. Res. **66**, 367 (1990).
[58]A. Vinet, "Quasiperiodic circus movement in a loop model of cardiac tissue: Multistability and low dimensional equivalence," Ann. Biomed. Eng. **28**, 704 (2000).
[59]D. Noble, "A modification of the Hodgkin-Huxley equations applicable to Purkinje fibre action and pacemaker potentials," J. Physiol. (London) **160**, 317 (1962).
[60]M. R. Guevara, L. Glass, and A. Shrier, "Phase locking, period-doubling bifurcations, and irregular dynamics in periodically stimulated cardiac cells," Science **214**, 1350 (1981).
[61]T. J. Lewis and M. R. Guevara, "Chaotic dynamics in an ionic model of the propagated cardiac action potential," J. Theor. Biol. **146**, 407 (1990).
[62]F. H. Fenton, S. J. Evans, and H. M. Hastings, "Memory in an excitable medium: A mechanism for spiral wave breakup in the low-excitability limit," Phys. Rev. Lett. **83**, 3964 (1999).
[63]G. M. Hall, S. Bahar, and D. J. Gauthier, "Prevalence of rate-dependent behaviors in cardiac muscle," Phys. Rev. Lett. **82**, 2995 (1999).
[64]I. Banville and R. A. Gray, "Effect of action potential duration and conduction velocity restitution and their spatial dispersion on alternans and the stability of arrhythmias," J. Cardiovasc. Electrophysiol. **13**, 1141 (2002).
[65]E. Cytrynbaum and J. P. Keener, "Stability conditions for the traveling pulse: Modifying the restitution hypothesis," Chaos **12**, 788 (2002).
[66]E. M. Cherry and F. H. Fenton, "Suppression of alternans and conduction blocks despite steep APD restitution: Electronic, memory, and conduction velocity restitution effects," Am. J. Physiol. Heart Circ. Physiol. **286**, H2322 (2004).
[67]S. Bauer, G. Röder, and M. Bär, "Alternans and the influence of ionic channel modifications: Cardiac three-dimensional and one-dimensional numerical bifurcation analysis," Chaos **17**, 015104 (2007).
[68]B. Echebarria and A. Karma, "Amplitude equation approach to spatial dynamics of cardiac alternans," Phys. Rev. E **76**, 051911 (2007).